OAK RIDGE
NATIONAL LABORATORY
MANAGED BY UT-BATTELLE
FOR THE DEPARTMENT OF ENERGY

ORNL/TM-2004/251

Modeling of the High Flux Isotope Reactor Cycle 400

N. Xoubi
R. T. Primm III

UT-BATTELLE
ORNL-27 (4-00)

ORNL/TM-2004/251

Research Reactors Division

MODELING OF THE HIGH FLUX ISOTOPE REACTOR CYCLE 400

N. Xoubi
R. T. Primm III

August 2005

Prepared by
OAK RIDGE NATIONAL LABORATORY
Oak Ridge, Tennessee 37831-6283
managed by
UT-BATTELLE, LLC
for the
U.S. DEPARTMENT OF ENERGY
under contract DE-AC05-00OR22725

CONTENTS

LIST OF FIGURES

LIST OF TABLES

ACKNOWLEDGMENTS

The authors would like to acknowledge the technical reviews of this document that were performed by J. C. Gehin and R. J. Ellis, both of Oak Ridge National Laboratory (ORNL). The author would also like to acknowledge the technical editing of C. C. Southmayd and the document preparation performed by B. J. Smith and F. G. Farrell, all of ORNL. Finally, the author wishes to acknowledge S. E. Burnette, ORNL, and the Oak Ridge Institute for Science and Education for providing programmatic support for this work.

The development of major portions of the computational model described in this report was initiated by L. A. Smith (formerly of ORNL, currently at Entergy Services, Inc.) and continued by J. C. Gehin of ORNL.

MODELING OF THE HIGH FLUX ISOTOPE REACTOR CYCLE 400

N. Xoubi
R. T. Primm III

ABSTRACT

For most of the operating life of the reactor, direct measurements or expert opinion based on past measurements have been the sources of data for the reactivity worth and heat generation rate of specimens to be irradiated in the reactor. With the current policy of the Department of Energy being to operate the High Flux Isotope Reactor (HFIR) to 2035 and with the goal of maximizing the reactor's capabilities and given the availability of sophisticated numerical analysis programs, a transition to computationally based estimates is believed to be the most economical and accurate practice for the future given that many of the individuals who performed the measurements are no longer employed at Oak Ridge National Laboratory. Computationally based estimates are believed to be less prone to error, that is, incorrect estimation of heating rates or reactivity, if the computational methodology is implemented correctly. This document was written for the purpose of insuring correct implementation and use of a computational model of the HFIR. A model of the reactor for use with the Monte Carlo N-Particle (MCNP) computer program is described and compared to the actual reactor configuration.

1. INTRODUCTION

One of the uses of the High Flux Isotope Reactor (HFIR) is to irradiate materials for medical or industrial applications. For each specimen to be irradiated, the nuclear heat generation rate and reactivity worth must be estimated. Frequently, prediction of postirradiation isotopic contents of the specimens is also desired. For most of the operating life of the reactor, direct measurement or expert opinion based on past measurements have been the sources of this information. The HFIR has been in operation for 40 years, and all of the original staff and many of the "second-generation" staff have now retired; unfortunately, much of their knowledge left with them. With the current policy of the Department of Energy (DOE) to operate the reactor to 2035 and with the goal of maximizing the reactor's capabilities and given the availability of sophisticated numerical analysis programs, a transition to computationally based estimates is believed to be the most economical and accurate practice for the future and less prone to error, that is, incorrect estimation of heating rates or reactivity, if implemented correctly. This document was written for the purpose of ensuring correct implementation and use of a computational model of the HFIR.

Nuclear engineers and analysts have relied on computer modeling and simulation for many years to evaluate performance and safety-related parameters for neutronics, criticality safety, and reactor analyses. Monte Carlo N-Particle (MCNP) is a three-dimensional (3-D) general purpose code that can be used to simulate coupled neutron/photon/electron transport, including the capability to calculate eigenvalues for critical systems.[1,2,3] The base model described herein reflects the as-built configuration of the reactor and includes all redesign, modifications, and upgrades to HFIR that have occurred since its first approach to criticality in 1965. In that sense, it represents an update to a similar, recently completed study.[4]

The HFIR MCNP "input file" is explicitly modeled in six sections, each representing a part of the reactor. This approach facilitates modification of the input cards to reflect any changes to the model or future experimental rearrangements. Graphs generated by MCNP of the six regions are included in this report; in addition, corresponding actual photos or drawings are presented side-by-side. The complete MCNP input model is included on a compact disc (CD) as part of this report. The effects of cross-section dataset selection on reactor physics parameters are also illustrated as part of this work.

1.1 HFIR DESCRIPTION

The HFIR is a multipurpose isotope production and test reactor. With a rated power of 100 MW, and currently operating at 85 MW, HFIR produces the world's highest steady-state neutron thermal flux (2.6×10^{15} neutrons/ $cm^2 \cdot s$), making it a one-of-a-kind facility, worldwide.

The HFIR is a pressurized light-water-cooled and -moderated, flux-trap type reactor that uses highly enriched ^{235}U as the fuel. The reactor core (shown in Fig. 1) consists of a series of concentric annular regions, each approximately 61 cm high (fueled height is 51 cm). The center of the core is a 12.70-cm-diam cylindrical hole, referred to as the "flux trap," which contains 37 vertical experimental target sites.

Surrounding the flux trap are two concentric fuel elements separated by a water region. The inner element contains

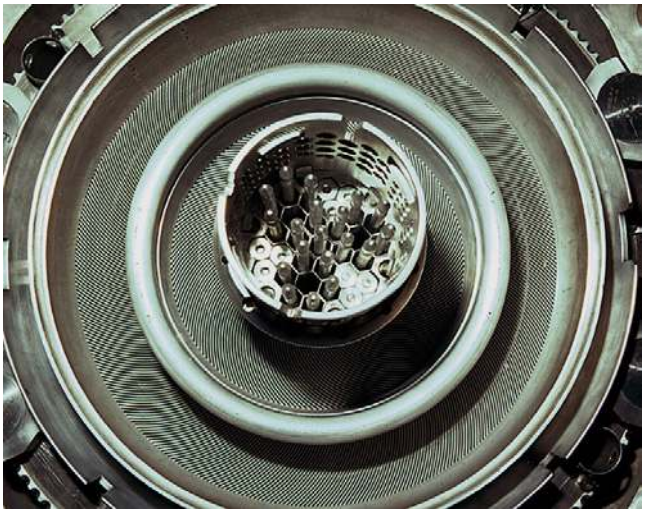

Fig. 1. The HFIR core, showing the inner and outer fuel elements and the flux trap region.

171 involute-shape fuel plates, and the outer element contains 369 involute-shape fuel plates. The fuel is aluminum-clad, highly enriched uranium oxide distributed along the arc of the involute aluminum plate (U_3O_8-Al cermet).

The inner fuel element contains boron (^{10}B) as a burnable poison, primarily to help shift the power distribution from the inner element to the outer element. The core loading is 9.4 kg of ^{235}U and 2.8 g of ^{10}B. The average core life cycle is 22–24 d at 85 MW (depending on quantity and type of material being irradiated).

The control plates, in the form of two thin, poison-bearing concentric cylinders, are located in an annular region between the outer fuel element and the beryllium reflector. These plates are driven in opposite directions. Reactivity is increased by downward motion of the inner cylinder, which is used only for shimming and regulation; that is, it has no fast safety function. The outer control cylinder consists of four separate quadrants, each having an independent drive and safety release mechanism. Reactivity is increased as the outer plates are raised. All control plates have three axial regions of different poison content designed to minimize the axial peak-to-average power-density ratio throughout the core lifetime. Any single rod or cylinder is capable of "shutting the reactor down".

The fuel region is surrounded by a concentric ring of beryllium that serves as a reflector and is approximately 30 cm thick. This, in turn, is subdivided into three regions: the removable reflector, the semipermanent reflector, and the permanent reflector, as shown in Fig. 2. The beryllium is surrounded by a water reflector of effectively infinite thickness. In the axial direction, the reactor is reflected by water.

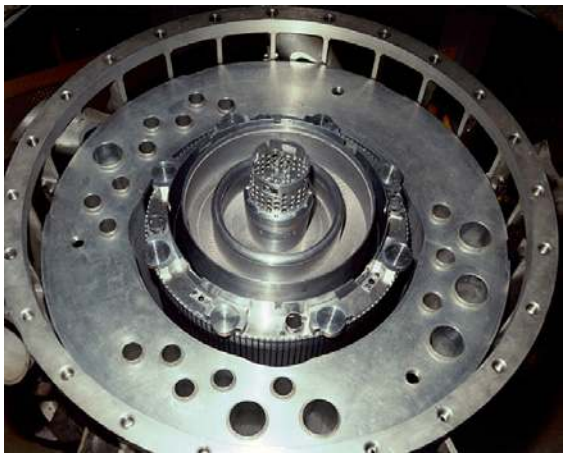

Fig. 2. The HFIR core with the beryllium reflector.

The reactor core assembly is contained in a 244-cm-diam steel pressure vessel located in a pool of water. The top of the pressure vessel is 518 cm below the pool surface, and the reactor horizontal midplane is 838 cm below the pool surface.

The control plate drive mechanisms are located in a sub-pile room beneath the pressure vessel. This feature provides the necessary shielding for working below the reactor core and greatly facilitates access to the pressure vessel, core, and reflector regions. A few key parameters of HFIR are presented in Table 1. Significant components of the reactor are identified in Fig. 3.

1.2 CYCLE 400

Cycle 400 started on April 27, 2004 at 2:55 a.m. The reactor operated at 85 MW until May 21, 2004, 5:35 p.m. Therefore, the life of cycle 400 was 24 d, 14 h, and 40 min, or 24.61 d.

The actual experimental loading of cycle 400 is shown in Fig. 4, and is described as follows:

A. Flux trap region:

- 21 solid aluminum dummy targets
- shrouded aluminum dummy targets
- stainless steel targets (JP-26 and 27)
- hydraulic tube (HT)
- peripheral target position (PTP) tubes (1 aluminum dummy)

B. Beryllium reflector: no experiments loaded.

Table 1. Key parameters of HFIR

Reactor power, MW	85	
Active core height, cm	50.8	
Number of fuel elements	2	
Fuel type	U_3O_8—aluminum	
Total ^{235}U loading, kg	9.43	
Enrichment, %	93.1	
Fuel element parameters	***Inner fuel element***	***Outer fuel element***
Number of fuel plates	171	369
^{235}U loading, kg	2.60	6.83
Average fuel uranium density, gU/cm^3	0.776	1.151
^{235}U per plate, g	15.18	18.44
Burnable poison in element (^{10}B), g	2.8	None
Fuel plate thickness, cm	0.127	0.127
Coolant channel between plates, cm	0.127	0.127
Minimum aluminum clad thickness, mm	0.25	0.25
Fuel plate width, cm	8.1	7.3
Fuel cycle length, d	~24	
Cycle 400 length, d	24.6	
Coolant inlet temperature, °F	120	
Coolant outlet temperature, °F	169	
Fuel plate centerline temperature, °F	323	

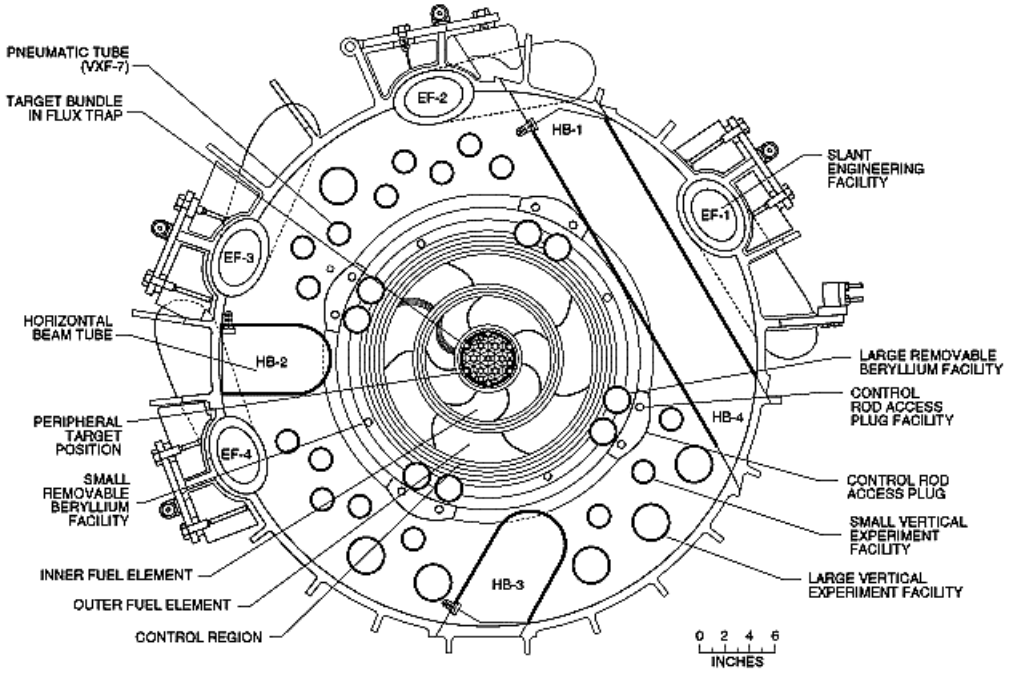

Fig. 3. Cross section of reactor core at horizontal midplane.

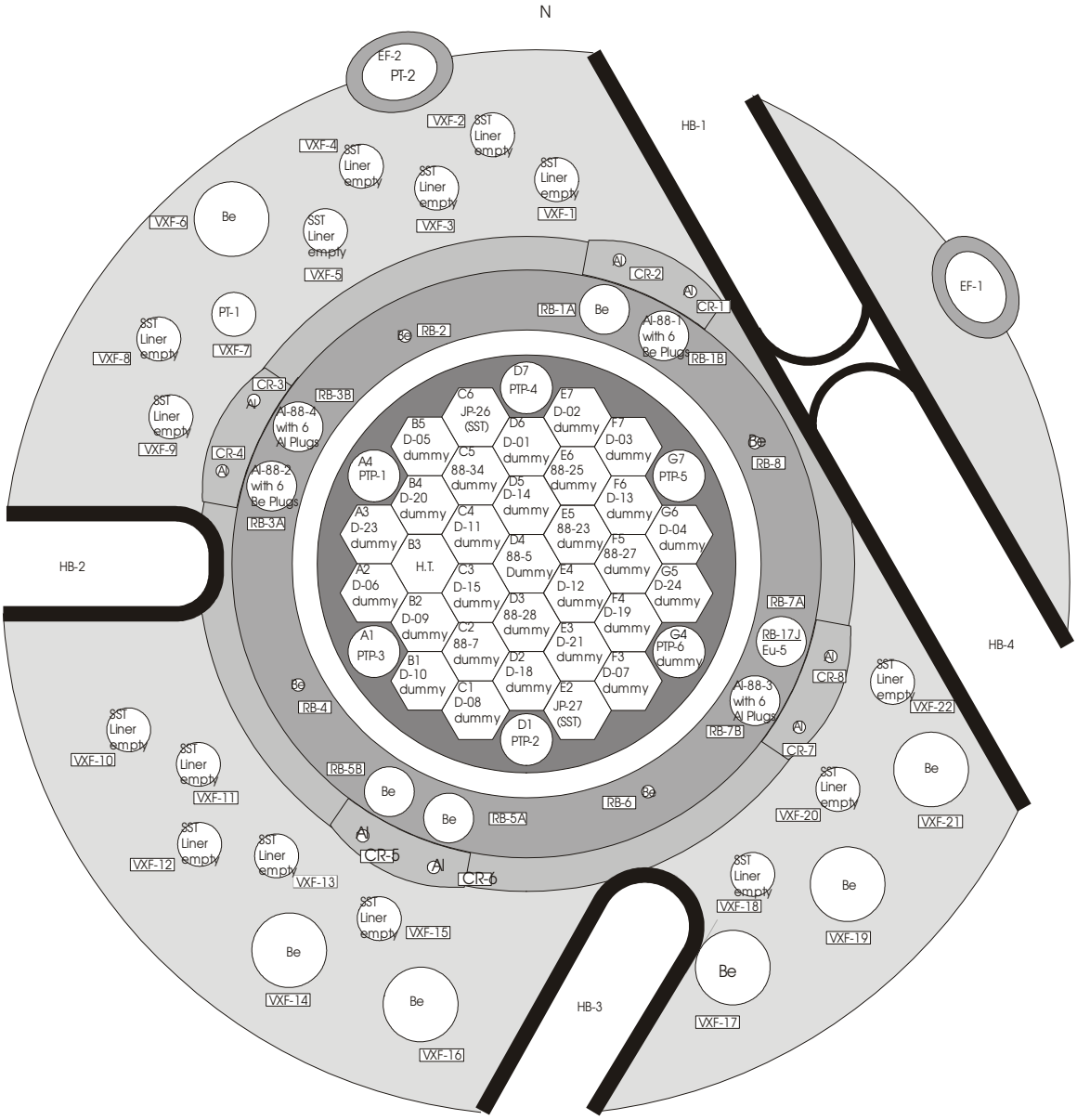

Fig. 4. Actual experimental loading of HFIR operating cycle 400 (drawing not to scale).

2. HFIR MODEL VERSION 4.0

HFIR model version 4.0 (HFV4.0) is a newly modified 3-D MCNP model that reflects the latest changes, target loading, and redesign of the HFIR core. It is based on an older model that was developed at ORNL, referred internally to ORNL as HFIR-V.2. The HFV4.0 model uses continuous energy neutron ENDF/B-VI cross-section data libraries.

The MCNP model for the HFIR is divided into six regions (parts), as follows:

- Region 1 is the flux trap target region (FTT),
- Region 2 is the inner fuel element region (IFE),
- Region 3 is the outer fuel element region (OFE),

- Region 4 is the control element region (CR),
- Region 5 is the removable reflector region (RB), and
- Region 6 is the beryllium permanent reflector region.

To make future changes, actual or proposed, easier to incorporate into the model, *cell* cards, *surface* cards, and *parameter* cards that effect the change in each region are marked for each region.

The HFV4.0 model is an explicit representation of the reactor, and every effort was made to make the model agree as closely as possible to operating cycle 400. A representation of the model is shown in Fig. 5. Cycle 400 was chosen because it was the reactor operating cycle at the time this model was being developed.

At the end of the MCNP dataset that is included with this report, additional information is provided. This information consists of data that are not used explicitly in this model. However, these data were employed in older models; therefore, they constitute valuable information that may be used again in the future and are thus archived within this report.

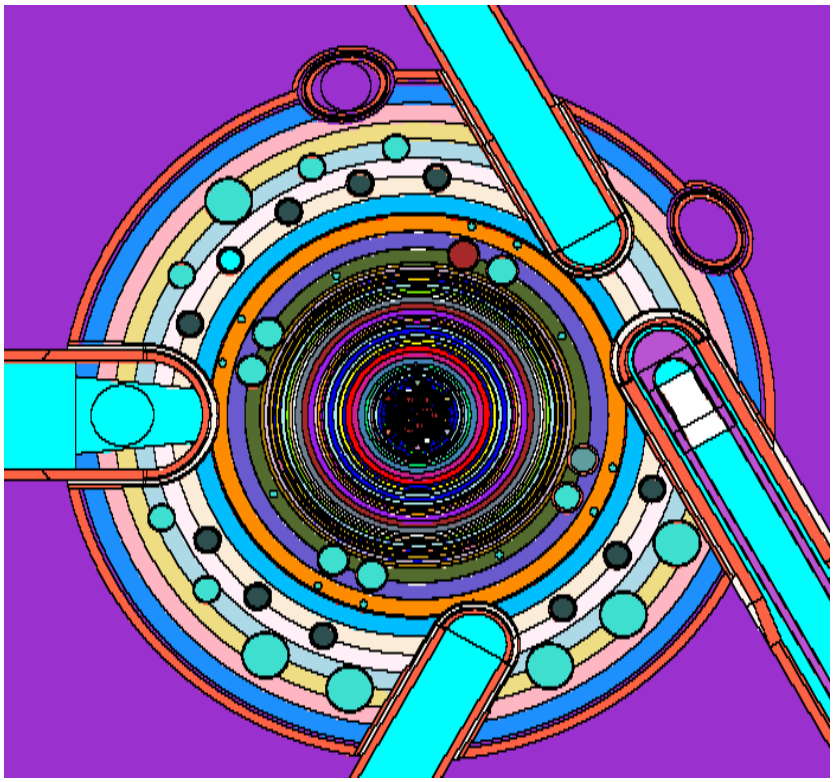

Fig. 5. MCNP model, cross section of reactor core at horizontal midplane (x-y).

2.1 NEUTRON CROSS SECTION DATA

The HFV4.0 model is based on the most recent continuous energy neutron cross section data from several libraries. For most materials in the code, the ENDF/B-VI.6 data library is used. The available data are evaluated at 293.6K, which is a good approximation of the HFIR reactor temperature. The source of the neutron cross section data (library) has an effect on calculational results. Thus, the various sources of neutron cross sections used in this model are presented in Table 2 for the convenience of the reader.

2.2 FLUX TRAP TARGET REGION (FTT)

The FTT region has 37 experimental sites; 31 sites are located in the interior of the basket, and 6 sites on the periphery of the basket—peripheral target positions (PTP)—as shown in Fig. 5. The target region was designed for rods containing ^{242}Pu as target material for producing californium. Shortly after startup of the reactor, sufficient quantities of curium became available for use as target material. One location contains a hydraulic tube and allows for insertion of specimens while the reactor is operating. When californium-production targets are not available for loading to the central target region, these locations are occupied by aluminum "dummy" targets. These may be either solid aluminum rods filling the region intended to be occupied by californium targets or shrouded aluminum rods. The shrouded rods contain a small diameter core and are vented to allow water ingress to the region between the core and shroud.

The cycle 400 experimental loading in the FTT was:

- 7 solid aluminum dummy targets (brown regions in Fig. 6),
- 21 shrouded aluminum dummy targets (target locations in Fig. 6 are orange with green rings surrounded by blue annuli),
- 2 stainless steel targets—designated JP-26 and -27 (solid green circles in Fig. 6),
- 1 hydraulic tube (HT; locations in Fig. 6 containing purple, burgundy, and green concentric annuli), and
- 6 PTP tubes (different colors located on the periphery at 60^{o} intervals).

Table 2. Neutron cross-section data used in MCNP model

Source file	Nuclide ID	Comment	MAT number	Creation date
endf66a	1001.66c	H-1 at 293.6K from endf-vi.6 (MOD) njoy99.50	125	07/18/01
	2003.66c	He-3 at 293.6K from endf-vi.1 njoy99.50	225	07/13/01
	3006.66c	Li-6 at 293.6K from endf-vi.1 njoy99.50	325	07/13/01
	4009.66c	Be-9 at 293.6K from endf-vi.0 njoy99.50	425	07/13/01
	5010.66c	B-10 at 293.6K from endf-vi.1 njoy99.50	525	07/13/01
	5011.66c	B-11 at 293.6K from endf-vi.0 (MOD) njoy99.50	528	07/18/01
	8016.66c	O-16 at 293.6K from endf-vi.6 njoy99.50	825	07/13/01
	13027.66c	AL-27 at 293.6K from endf-vi.6 njoy99.50	1325	07/24/01
rmccs	6012.50c	16126 njoy	—	79/07/31
	24000.50c	89104 njoy	—	79/06/21
	28000.50c	82267 njoy	—	79/06/21
	29000.50c	22473 njoy	—	02/05/80
actia	12000.62c	Mg at 293.6K from endf/b-vi.8 njoy99.50	1200	12/06/01
	22000.62c	Ti at 293.6K from endf/b-vi.8 njoy99.50	2200	12/06/01
	25055.62c	Mn-55 at 293.6K from endf/b-vi.8 njoy99.50	2525	02/11/02
endf60	14000.60c	Si from endf/b-vi	1400	11/25/93
100xs	26000.21c	Fe- from pgy 100 MeV library (fe100n6)	260	09/01/95
endl92	63000.42c	Eu ENDL library name: nd920609	—	—
endf66b	63151.66c	Eu-151 at 293.6K from endf-vi.0 njoy99.50	6325	08/10/01
	63153.66c	Eu-153 at 293.6K from endf-vi.0 joy99.50	6331	08/10/01
	73181.66c	Ta-181 at 293.6K from endf-vi.0 njoy99.50	7328	02/13/02
endf66c	92234.66c	U-234 at 293.6K from endf-vi.0 njoy99.50 total nu	9225	08/13/01
	92235.66c	U-235 at 293.6K from endf-vi.5 njoy99.50 total nu	9228	08/14/01
	92236.66c	U-236 at 293.6K from endf-vi.0 njoy99.50 total nu	9231	09/05/01
	92238.66c	U-238 at 293.6K from endf-vi.5 njoy99.50 total nu	9237	08/14/01
Tmccs	be.60t	10224 beryllium metal at 300K	—	10/24/85
	lwtr.60t	10193 hydrogen in light water at 300K	—	10/22/85

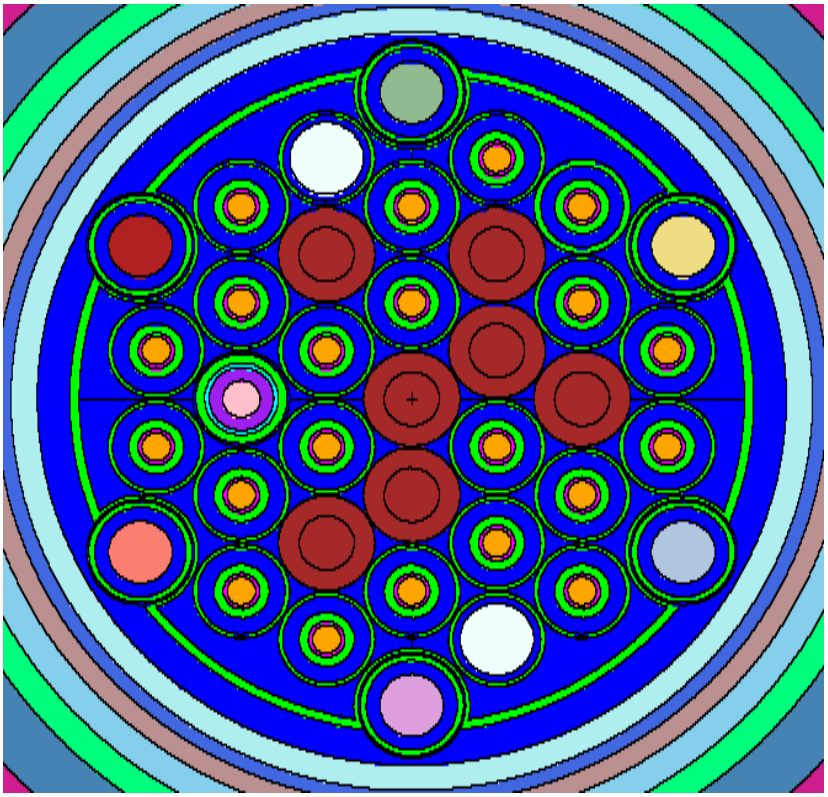

Fig. 6. Horizontal view of the flux trap region as modeled in HFV4.0.

Cycle 400 was mostly loaded with dummy targets; in fact, 28 of the 37 experimental sites in the flux trap region were filled with dummy aluminum targets, both solid and shrouded.

Figure 7 shows the original target configuration at the time the HFIR first went critical in 1965. Note that the hydraulic tube was located at the center of the target region at that time. Figure 7 is included because the identification scheme identified in the figure is still used today.

2.2.1 JP-26 and JP-27

JP-26 and JP-27 rods are located in C6 (see Fig. 7) and E2 experimental sites, respectively. The targets are solid stainless steel in an aluminum holder.

The target region of the holder was modeled by homogenizing the stainless steel and aluminum over that whole volume. The upper and lower parts of the holder are aluminum and were modeled as such.

The outer shroud is also aluminum and was modeled as a cylindrical aluminum tube. The coolant around the holder and outside the shroud was modeled as such, with the material being water at the core operating temperature and pressure, that is, a density of 0.98465 g/cm^3. The portions of the MCNP dataset that represent this region are shown in Fig. 8 and pictorially represented in Fig. 9. Note, though, that for this figure and other, succeeding figures, the surface "cards" are not shown. The user is referred to the HFV4.0 dataset for the surface cards.

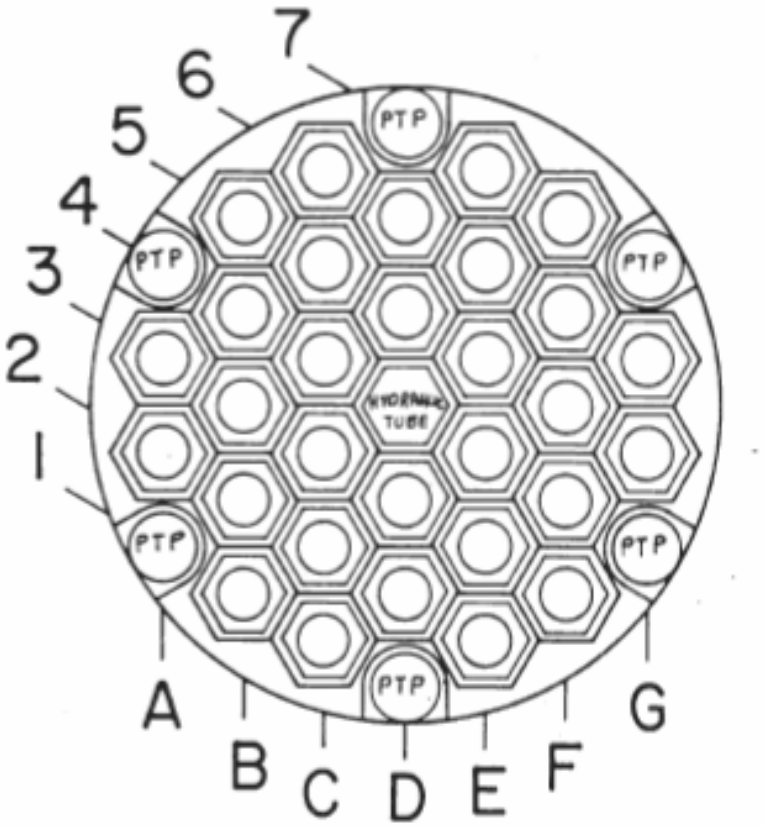

	Radial Distance Reactor Vertical Centerline (cm)
C3, C4, D3, D5, E4, E5	1.689
B3, C2, C5, E3, E6, F5	2.926
B2, B4, D2, D6, F4, F6	3.378
A2, A3, B1, B5, C1, C6, E2, E7, F3, F7, G5, G6	4.465
A1, A4, D1, D7, G4, G7	5.067

Fig. 7. HFIR central target position identification scheme.

```
c
c     ***** E-2  (JP-27 SST-304  targets)
c    Jp-26 & Jp-27 solid SSt targets in Al holders
c
610   535 5.97-02  -612 +427 -428  imp:n=1  $ sst targets in Al holder
612   25 6.02083-02 #(-612 +427 -428) -612 +417 -419  imp:n=1 $ Holder upper & lower regions
613   25  6.02423-02   +613 -614  -418 +416    imp:n=1      $ outer shroud Al
614   2     9.95227-02      612 -613  +417 -419   imp:n=1            $ coolant
615   2     9.95227-02      #613 613 -615  +417 -419    imp:n=1      $ coolant
c
c
c
c  Material for Jp-26 & Jp-27 solid SSt targets in Al holders Total = 5.97E-02 m535       13027.66c
3.22-02
         26000.55c   1.89E-02
         24000.50c   5.55E-03
         28000.50c   2.46E-03
         25055.60c   5.53E-04
c
c
```

Fig. 8. Portion of MCNP input dataset that represents JP-26 and JP-27 targets.

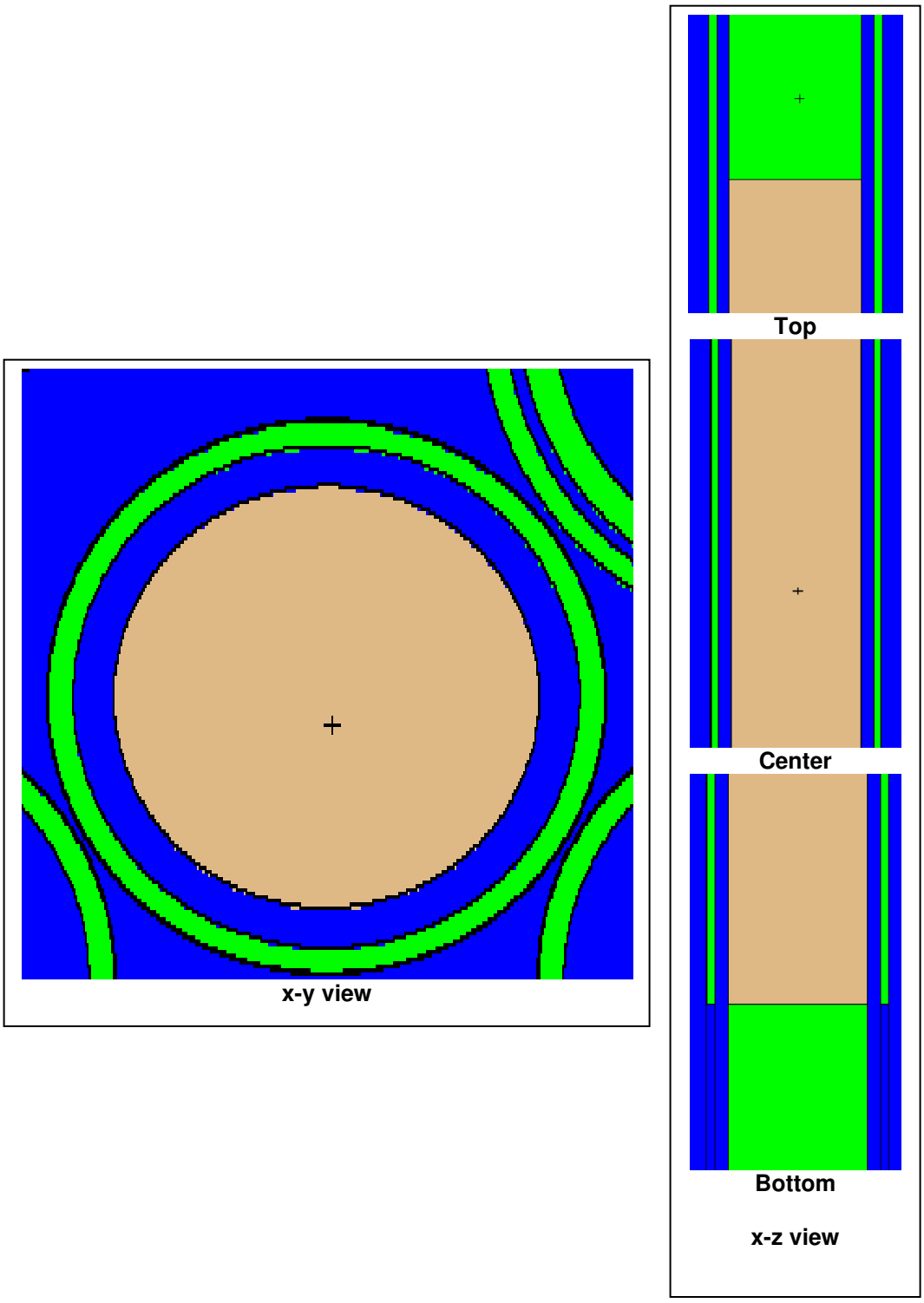

Fig. 9. HFV4.0 MCNP modeling of JP-26 experiment loading located in C6 experimental sites.

2.2.2 Hydraulic Tube

The hydraulic tube (HT) is located in the site designated as B3 (see Fig. 7, not the location designated in Fig. 7 as "hydraulic tube;" that being the original site at reactor start-up). For the current capsule design, the tube can be loaded with nine specimens, frequently designated "rabbits." The HT is explicitly modeled for the nine experiment locations and its experimental targets. Material definition for different experimental targets can easily be input to the model. The portions of the MCNP dataset that represent this region are shown in Fig. 10 and pictorially represented in Fig. 11.

```
c        ***** B-3 The hydraulic tube (HT)
c
750      520   6.02423–02    –450 + 752   –751      imp:n=1    $ target material upper target
751      520   6.02423–02    –450 + 755   –754      imp:n=1    $ target material
752      520   6.02423–02    –450 + 758   –757      imp:n=1    $ target material
753      520   6.02423–02    –450 + 761   –760      imp:n=1    $ target material
754      520   6.02423–02    –450 + 764   –763      imp:n=1    $ target material centerline target
755      520   6.02423–02    –450 + 767   –766      imp:n=1    $ target material
756      520   6.02423–02    –450 + 770   –769      imp:n=1    $ target material
757      520   6.02423–02    –450 + 773   –772      imp:n=1    $ target material
758      520   6.02423–02    –450 + 776   –775      imp:n=1    $ target material lower target
c
760      521   6.02423–02    –451 + 753   –750 (450:–752:751)   imp:n=1   $ target tube upper target
 761     521   6.02423–02    –451 + 756   –753 (450:–755:754)   imp:n=1   $ target tube
762      521   6.02423–02    –451 + 759   –756 (450:–758:757)   imp:n=1   $ target tube
763      521   6.02423–02    –451 + 762   –759 (450:–761:760)   imp:n=1   $ target tube
764      521   6.02423–02    –451 + 765   –762 (450:–764:763)   imp:n=1   $ tube centerline target
 765     521   6.02423–02    –451 + 768   –765 (450:–767:766)   imp:n=1   $ target tube
766      521   6.02423–02    –451 + 771   –768 (450:–770:769)   imp:n=1   $ target tube
 767     521   6.02423–02    –451 + 774   –771 (450:–773:772)   imp:n=1   $ target tube
768      521   6.02423–02    –451 + 777   –774 (450:–776:775)   imp:n=1   $ target tube lower target
c
452      60    2.00000–15    –452 + 451    +777    –750    imp:n=1   $ air space
453      25    6.02083–02    –453 + 452    +777    –750    imp:n=1   $ outer clad
454      2     9.95227–02    –454 + 453    +777    –750    imp:n=1   $ coolant
c
455      25    6.02083–02    –453 + 417    –777    imp:n=1     $ Al block—below core
456      2     9.95227–02    –454 + 453    +417    –777        imp:n=1      $ coolant—below core
c
446      60    2.00000–15    –451 + 750    –419    imp:n=1   $ target and tube—above targets (air)
447      60    2.00000–15    –452 + 451    +750    –419      imp:n=1      $ air space—above core
448      25    6.02083–02    –453 + 452    +750    –419      imp:n=1      $ outer clad—above core
449      2     9.95227–02    –454 + 453    +750    –419      imp:n=1      $ coolant—above core
C
```

Fig. 10. Portion of MCNP input dataset that represents the hydraulic tube.

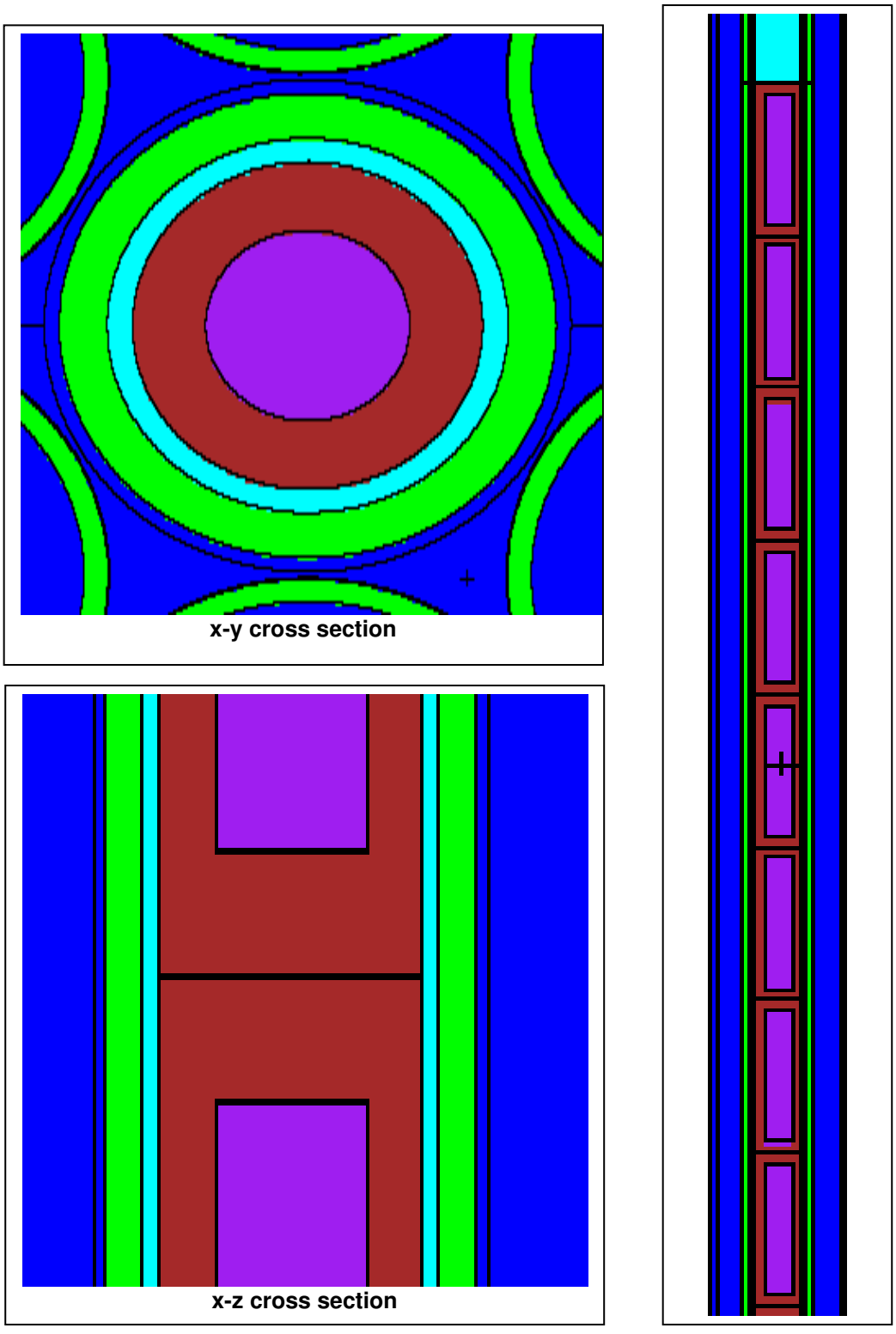

Fig. 11. HFV4.0 MCNP modeling of HT-located in B3 experimental sites.

2.2.3 Peripheral Target Positions (PTP)

The target region contains six PTP sites; these are symmetrically located on the periphery of the target basket. The contents of the PTP positions for cycle 400 are provided in Table 3. Boundaries of the seven axial regions described in Table 3 are provided in Table 4. Each capsule shown in Table 3 has a volume of 6.53034 cm^3. The PTPs were explicitly modeled with the MCNP input lines shown in Fig. 12, and a pictorial representation of location D7 is shown in Fig. 13.

```
c     ***** PTP-2  (D-1)
c
821   721  5.65355-02 -940 +970 -971 imp:n=1 $ First capsule (bottom)
822   722  6.00000-02  -940 +971 -972  imp:n=1  $ Second target capsule
823   723  5.93745-02  -940 +972 -973  imp:n=1  $ Third target capsule
824   724  5.89491-02  -940 +973 -974  imp:n=1  $ Fourth target capsule
825   725  5.89252-02  -940 +974 -975  imp:n=1  $ Fifth target capsule
826   726  5.93745-02  -940 +975 -976  imp:n=1  $ Sixth target capsule
827   727  6.03159-02  -940 +976 -977  imp:n=1  $ Seventh capsule (Top)
c
940   25  6.02083-02  -940 +977 -909   imp:n=1    $ clad upper region
941   25  6.02083-02  -940 +908 -970   imp:n=1    $ clad lower region
942   25  6.02083-02  +942 -943  +907  -909   imp:n=1    $ outer shroud
943   2  9.95227-02   +940 -944  +908  -909
(-942:943:-907)    imp:n=1    $ coolant
944   2  9.95227-02   -944  +909  -419   imp:n=1    $ coolant (above)
945   2  9.95227-02   -944  +417  -908   imp:n=1    $ coolant (below)
c
c   #1  (bottom) experiment material   Gr/Al     Total=5.65355-2
m721   13027.66c  0.0285703  14000.60c  0.0004611   26000.55c  0.0008843
       42000.66c  0.0003489  6000.66c  0.0262709
mt721      grph.60t
c
c   #2  experiment material   SiC/V     Total = 4.34300-2
m722     13027.66c   0.0174491   14000.60c  0.0114365
         6000.66c  0.0114365      26000.55c  0.0008035
         42000.66c  0.0001735    23000.66c  0.0135674
mt722    grph.60t
c
c   #3  experiment material (s1) Al spacer Al-1100  Total =  5.93745-02
m723   13027.66c 6.00625-02  14000.60c 1.45271-04  25055.60c 7.42655-06
       26000.55c   7.30588-05  29000.50c   3.57670-05
c
c   #4  experiment material   Gr/V     Total = 5.89491-2
m724   13027.66c 0.0175354   14000.60c 0.0004705    26000.55c  0.0008799
       42000.66c 0.0003048   6000.66c  0.0262254    23000.66c  0.0135332
mt724      grph.60t
c
```

Fig. 12. Portion of MCNP input dataset that represents the peripheral target positions.

Table 3. PTP loading cycle 400

Pos: A-4	1(bottom)	2	3	4	5	6	7(top)
Contents: Cycle 400 PTP-1	S-19 Aluminum Spacer	1-04-3 SO3-003 SST/Al 399/406	4-04-2 NM-634 W 400/400	4-04-1 NM-627 W 400/400	11-02-04 S2 Mo/V 391/410	12-03-6 NM-659 Ra 398/400	5-03-14 T031 (5) SST Tensile 395/400
Atom density [#/(bn*cm)]	Al 0.059374	Al 0.035626 Mo 0.000173 Si 0.000305 Fe 0.008229 C 0.000406	W-186 0.001024 O 0.002096 Al 0.030701	W-186 0.000954 O 0.001972 Al 0.030701	V 0.017243 Mo 0.005969	Ra-226 1.54E-07 O 1.26E-07 Al 0.035052	Fe-54 0.000392 Fe-56 0.005928 Fe-57 0.000134 Fe-58 1.76E-05

Pos: D-1	1(bottom)	2	3	4	5	6	7(top)
Contents: Cycle 400 PTP-2	1-04-07 LO3115 Gr/Al 399/404	5-03-05 F0364 SiC/V 394/400	S-3 Aluminum Spacer	1-04-13 LO3125 Gr/V 399/400	1-04-14 LO3126 Gr/V 399/400	S-21 Aluminum Spacer	1-04-10 LO3120 Gr/V 399/400
Atom density [#/(bn*cm)]	AL 0.02857 Si 0.000461 Fe 0.000884 Mo 0.000349 C 0.026271	Al 0.017449 Mo 0.000174 Si 0.011437 Fe 0.000804 C 0.011437 V 0.013567	0.0593 Al 74	AL 0.017535 Si 0.00047 Fe 0.00088 Mo 0.000305 C 0.026225 V 0.013533	AL 0.017462 Si 0.000469 Fe 0.000877 Mo 0.000357 C 0.026264 V 0.013495	Al 0.059374	AL 0.017475 Si 0.000469 Fe 0.00089 Mo 0.00034 C 0.026355 V 0.014786

Pos: A-1	1 (bottom)	2	3	4	5	6	7(top)
Contents Cycle 400 PTP-3	1-04-08 LO3116 Gr/Al 399/404	5-03-02 F0363 (7) SiC/V 394/400	S-xx Aluminum Spacer	11-02-6 S4 (20) Mo/V 391/410	11-02-5 S1 (20) Mo/V 391/410	S-18 Aluminum Spacer	1-04-11 LO3121 Gr/V 399/402
Atom density [#/(bn*cm)]	AL 0.028524 Si 0.000469 Fe 0.000894 Mo 0.000357 C 0.02616	Al 0.017449 Mo 0.000174 Si 0.011199 Fe 0.000804 C 0.011199 V 0.013558	Al 0.059374	V 0.019983 Mo 0.005972	V 0.017262 Mo 0.005969	Al 0.059374	AL 0.017418 Si 0.000461 Fe 0.000887 Mo 0.000342 C 0.026012 V 0.014778

Table 3. (continued)

Pos: D-7	1(bottom)	2	3	4	5	6	7(top)
Contents: Cycle 400 PTP-4	1-04-6 LO3114 Gr/Al 399/401	5-03-07 F0365 (7) SiC/V 394/400	S-16 Aluminum Spacer	12-03-1 L03F7 Mo/Al 398 / 400	12-03-2 L03F8 Mo/Al 398/400	S-23 Aluminum Spacer	1-04-9 LO3119 Gr/V 399/400
Atom density [#/(bn*cm)]	C 0.043066 Al 0.036143 Si 0.002433	Al 0.017449 Mo 0.000174 Si 0.011078 Fe 0.000804 C 0.011078 V 0.01362	Al 0.059374	Al 0.043212 Fe 0.000221 Mo 0.00556	Al 0.043332 Fe 0.000221 Mo 0.005526	Al 0.059374	AL 0.017502 Si 0.000461 SS Fe 0.000884 Mo 0.000356 C 0.025817 V 0.014787

Pos: G-7	1(bottom)	2	3	4	5	6	7(top)
Contents: Cycle 400 PTP-5	S-4 Aluminum Spacer	5-03-09 F0366 SiC/V 394/400	4-04-08 LO3-106 400/404	4-04-7 LO3-100 400/401	4-04-6 LO3-101 400/401	S-9 Aluminum Spacer	1-04-12 LO3122 Gr/V 399/402
Atom density [#/(bn*cm)]	Al 0.059374	Al 0.017449 Mo 0.000174 Si 0.011297 Fe 0.000804 C 0.011297 V 0.013556	Al 0.041717 Fe 0.000221 Mo 0.00556	Si 0.014597 C 0.014595 Al 0.021686 V 0.019159	Si 0.014597 C 0.014595 Al 0.021686 V 0.019159	Al 0.059374	AL 0.017485 Si 0.000469 SS Fe 0.000892 Mo 0.000338 C 0.026047 V 0.014801

Pos: G-4	1(bottom)	2	3	4	5	6	7(top)
Contents: Cycle 400 PTP-6	1-04-5 LO3113 Gr/Al 399/401	1-04-1 SO3-001 SST/Al 399/406	1-04-2 SO3-002 SST/Al 399/406	1-04-15 LO3127 Gr/V 399/401	1-04-16 LO3128 Gr/V 399/401	S-20 Aluminum Spacer	4-04-05 LO3075 400/400
Atom density [#/(bn*cm)]	AL 0.028479 Si 0.000468 Fe 0.000879 Mo 0.000299 C 0.026209	AL 0.035837 Si 0.000305 Fe 0.008205 Mo 0.00018 C 0.000406	AL 0.035837 Si 0.000305 SS Fe 0.003559 Mo 0.000173 C 0.000406	Si 0.002433 C 0.043066 Al 0.0253 V 0.017243	Si 0.002433 C 0.043066 Al 0.0253 V 0.017243	Al 0.059374	AL 0.041717 SS Fe 0.000221 Mo 0.00556

Table 4. MCNP model boundaries corresponding to PTP positions

Table 3 zone number	Lower boundary (cm; 0.0 is axial midplane of reactor core)
1	–25.00
2	–18.47
3	–11.94
4	–5.41
5	1.12
6	7.65
7	14.18
(top of 7)	20.71

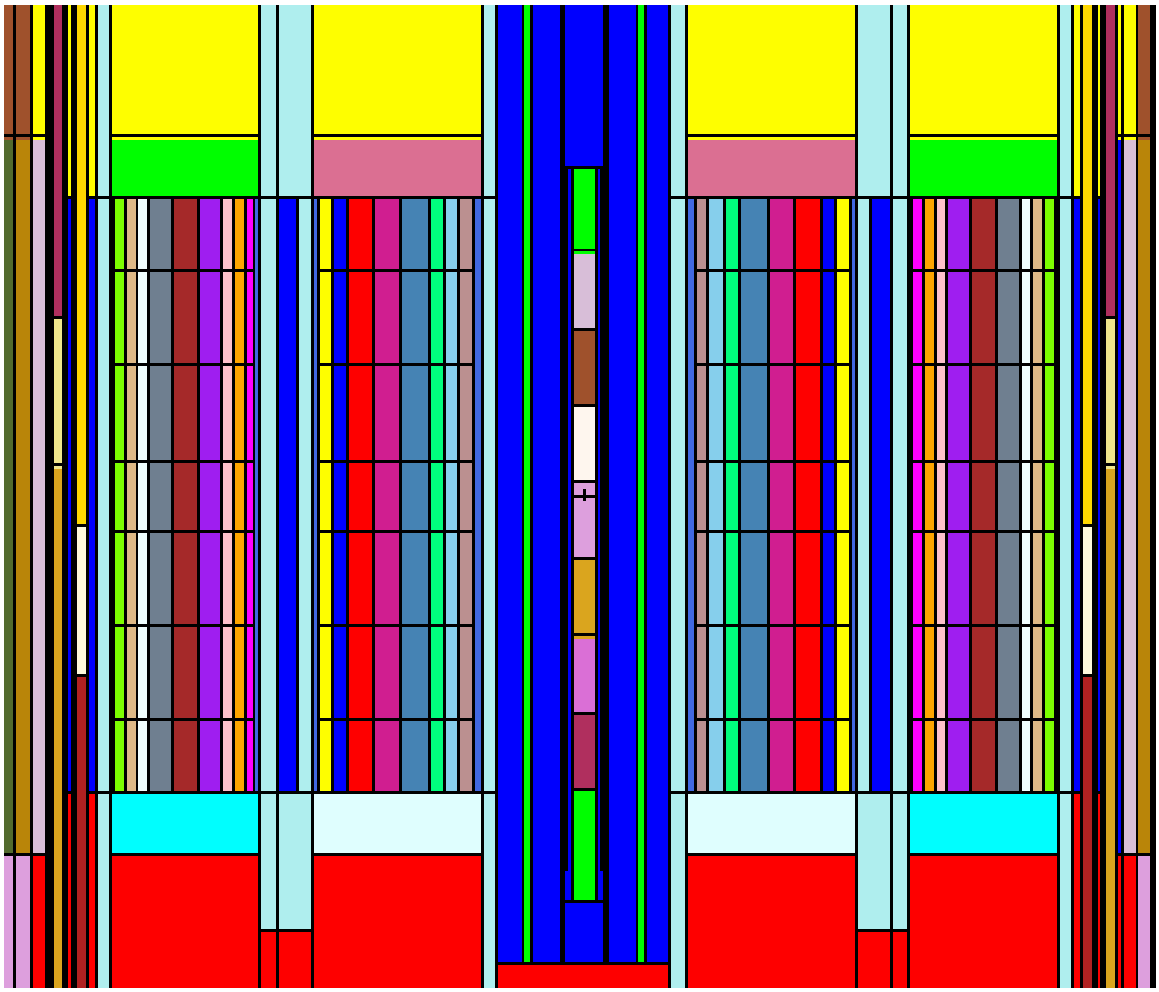

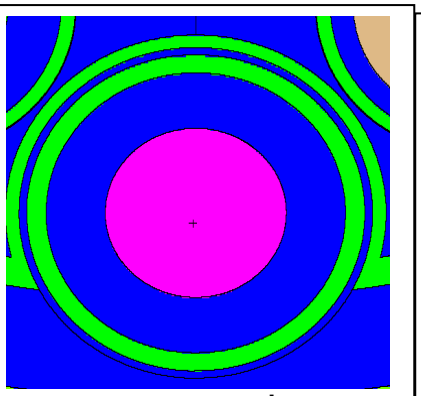

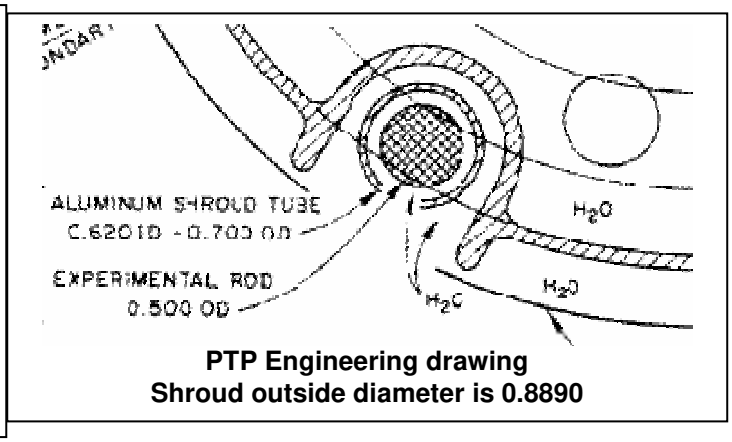

Fig. 13. HFV4.0 MCNP modeling of PTP2 located in D1 experimental sites.

2.2.4 Solid Aluminum Target Rod

Solid aluminum rods are loaded as "dummy" experimental targets in the flux trap region. They are loaded in unused target sites to maintain proper coolant flow in the target region and to provide a support structure for other target rods. A maximum of ten solid aluminum rods can be loaded in the target region due to the fact that the presence of solid aluminum rods increases the flow rate in shrouded rods in the target region (note water flow paths inside shrouded rods in Fig. 6). If greater than ten rods were loaded, it is speculated that the increased flow rate could lead to flow-induced vibration in the shrouded tubes with consequent erosion of target rods. Aluminum is used because of its transparency to neutrons (very low neutron absorption cross section) and thus provides a minimal perturbation of the flux in that region.

Cycle 400 contained seven solid aluminum targets, located at the following experimental sites: C2, C5, D3, D4, E5, E6, F5. The targets were modeled as pure aluminum. Figure 14 shows that portion of the MCNP input file corresponding to the solid aluminum target, and Fig. 15 provides a pictorial representation.

```
c
c    ***** C-2  (solid Al dummy)
490   530   6.02423-02   -492  +417 -419  imp:n=1 $ solid Al dummy outer clad and upper & lower regions
491   530  6.02423-02  +492 -494  -418 +416  imp:n=1 $ solid Al dummy outer shroud
492   2   9.95227-02   #491 +492 -495 +417 -419  imp:n=1   $ coolant
C
c
c      Dummy solid Al targets  (Al-1100) Total = 6.03240-02
c
m530   13027.66c 6.00625-02  14000.60c 1.45271-04  25055.60c 7.42655-06
          26000.55c   7.30588-05  29000.50c   3.57670-05
c
c       Water in core region    --Avg. Density = 0.98465 g/cm^3
m2       1001.66c     6.63485-02    8016.66c    3.31742-02
mt2      lwtr.60t
c
```

Fig. 14. MCNP input corresponding to solid aluminum target.

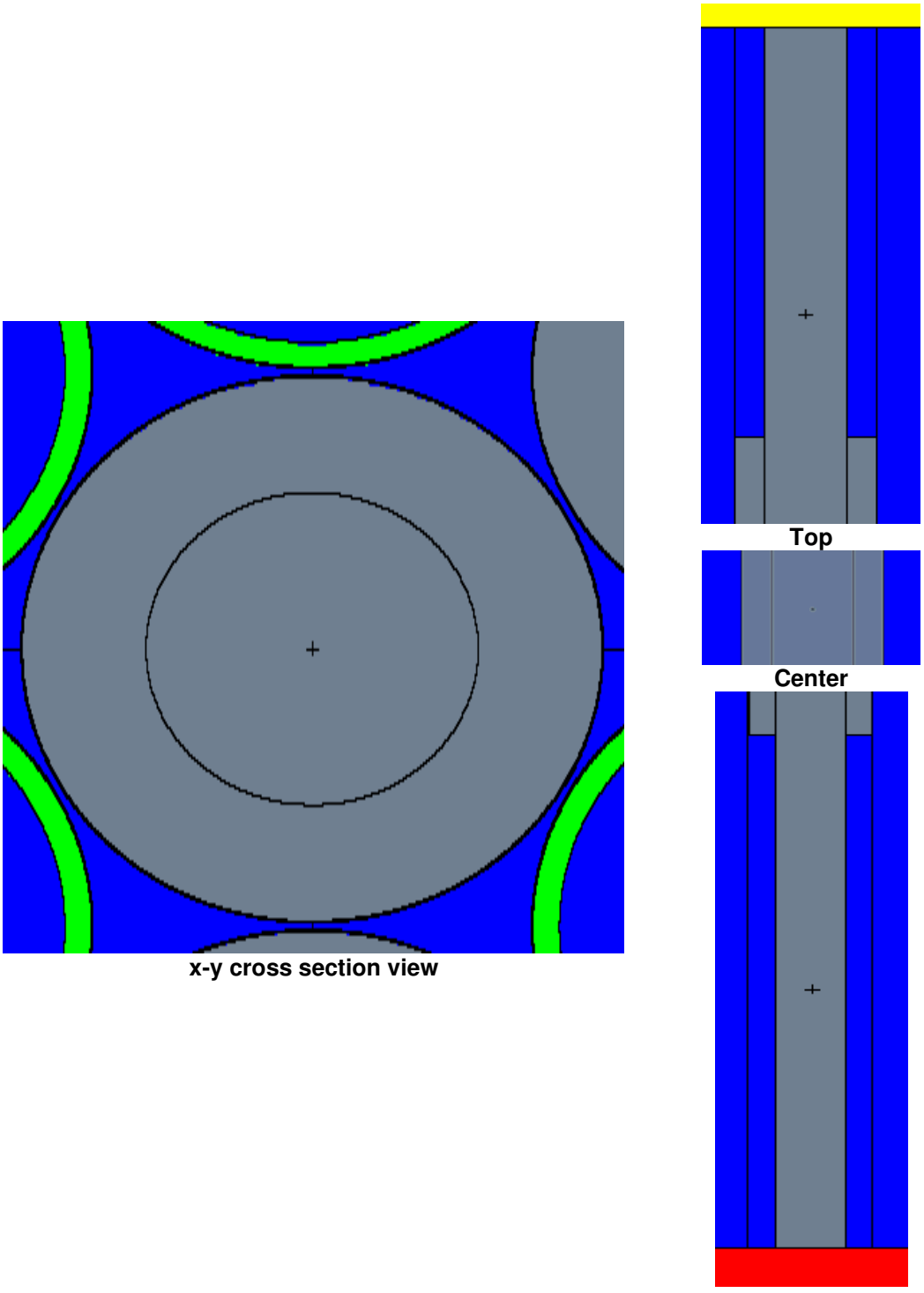

Fig. 15. HFV4.0 MCNP modeling of solid aluminum dummy targets loading located in seven different experimental sites.

2.2.5 Shrouded Aluminum Target Rod

Shrouded aluminum target rods, like solid aluminum rods, are loaded in unused target sites to maintain the proper coolant flow and to provide support structure for other target rods. The shrouded rods are configured to be geometric duplicates of the californium production rods and were the first "dummy" target rod design. Solid aluminum rods were designed at a later date due to unavailability of the manufacturing processes used for the shrouded aluminum rods.

Cycle 400 contained 21 shrouded aluminum dummy targets, located at the following experimental sites: A2, A3, B1, B2, B4, B5, C1, C3, C4, D2, D5, D6, E3, E4, E7, F3, F4, F6, F7, G5, and G6. The MCNP model for the aluminum shrouded rods is shown in Fig. 16. A pictorial representation is shown in Fig. 17.

```
c    ***** B-2  (shrouded Al dummy)
440   512  4.82102-02   –440 +427  –428            imp:n=1    $ dummy Al target material
441   511  6.03240-02   –441 +440  +427  –428     imp:n=1    $ dummy Al target tube
442   25  6.02083-02  #(–441 +427 –428) –442  +417  –419  imp:n=1 $ outer clad and upper & lower
regions
443   25  6.02083-02    +443 –444  +416  –418     imp:n=1    $ outer shroud
444   2  9.95227-02    +442 –445  +417  –419
                        (–443:444: –416:418)           imp:n=1    $ coolant
c

c       Al-1100 clad of target pellets       Total = 6.03240-02
m511     13027.66c   6.00625-02  14000.60c   1.45271-04  25055.62c   7.42655-06
           26000.21c   7.30588-05  29000.50c   3.57670-05
c
c       Al for shrouded targets (Al-1100) Total = 6.03240-02
m512    13027.66c   6.00625-02  14000.60c   1.45271-04  25055.60c   7.42655-06
           26000.55c   7.30588-05  29000.50c   3.57670-05
c
c
c       Aluminum in target basket area
m25      13027.66c   5.85482-02  1001.66c    3.45716-04 12000.62c    6.68986-04
           14000.60c   3.47363-04 22000.62c    2.54704-05 24000.50c    6.09789-05
           25055.62c   2.21974-05 26000.21c    1.01905-04 29000.50c    8.74557-05
c
```

Fig. 16. MCNP input corresponding to shrouded aluminum target rods.

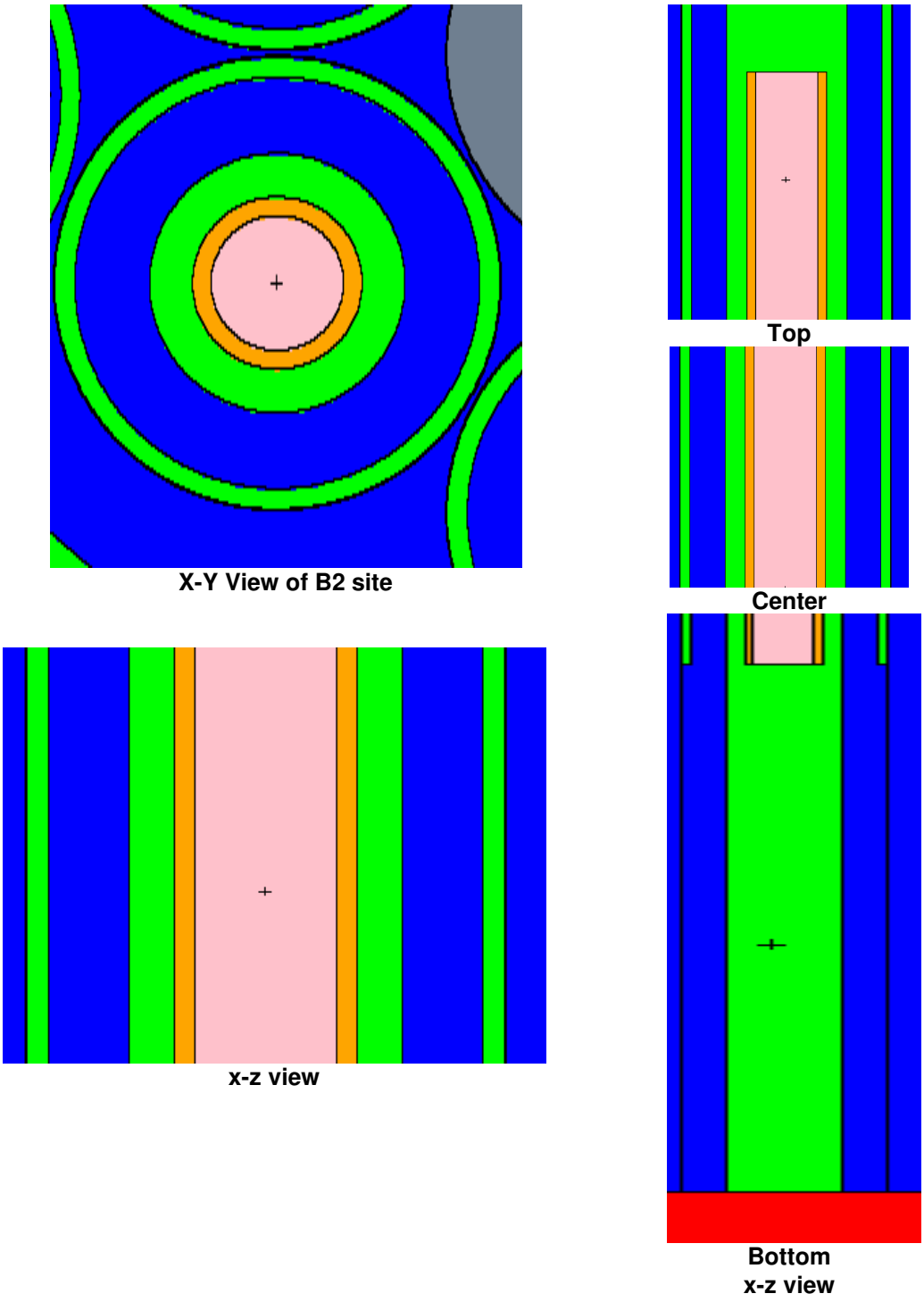

Fig. 17. MCNP modeling of the shrouded aluminum dummy targets.

2.2.6 Other Central Target Experiment Loadings

Other target experiment loadings that were not used in cycle 400, but are commonly used as targets in the HFIR follow:

- curium targets,
- 5% stainless steel (SST) experiment,
- 10% SST experiment,
- 20% SST experiment,
- 30% SST experiment,
- 40% SST experiment, and potentially,
- beryllium reflector rods.

The input files and material definitions for these loadings are included in the dataset on the CD that accompanies this report. The user can easily modify the model to reflect future loading of these experiments.

2.3 INNER FUEL ELEMENT

The inner fuel element (IFE) consists of 171 fuel plates; each plate formed in an involute shape. The fuel plates are U_3O_8-Al fuel meat with the uranium being highly enriched (93 wt. % ^{235}U). Each plate contains 15.18 g ± 1% of ^{235}U distributed along the involute arc in a varying thickness so as to reduce power peaking in the fuel plate (shown in Fig. 18) and clad with aluminum. The plates are separated by 50 one-thousandth inch gaps (filled with water during operation in the reactor), and are held in place by two cylindrical aluminum side walls.

The IFE fueled area is modeled by dividing it into 56 cells, 8 radial fuel regions and 7 axial fuel layers (Fig. 19).

The eight radial regions are included to approximate the varying, effective ^{235}U concentration in the radial direction of the fuel plate. The fuel is modeled by homogenizing the uranium "meat," aluminum, and water between the plates into eight radial fueled regions.

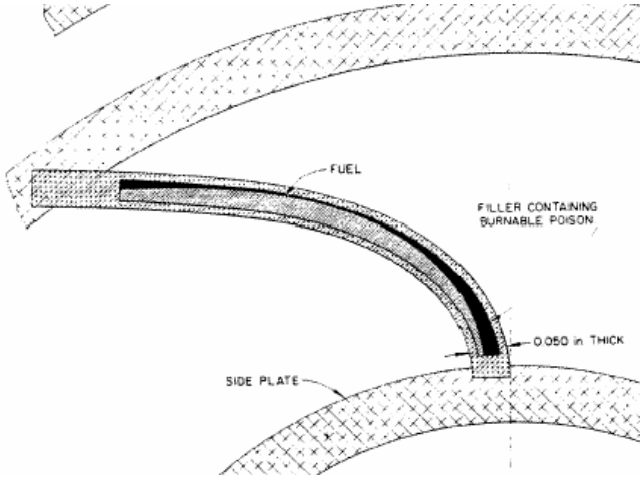

Fig. 18. IFE showing one plate with the fuel cladding, and the aluminum side plates holding the fuel plates together.

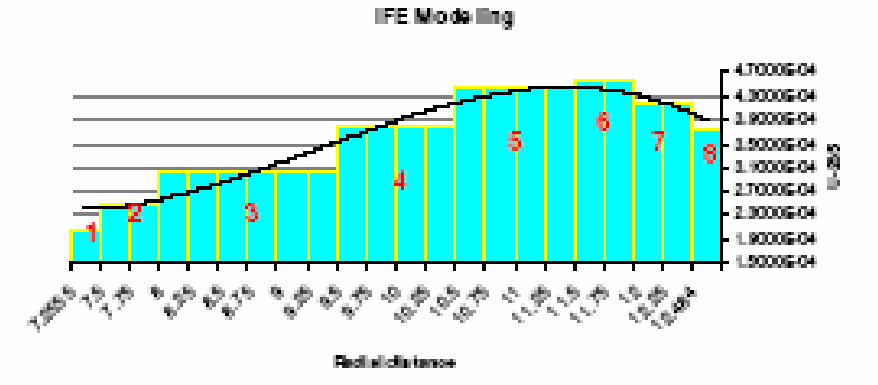

Fig. 19. Inner fuel element ^{235}U concentration and radial modeling.

The unfueled region of the IFE is modeled by homogenizing the aluminum and water. Figure 20 shows a cross section view of the IFE at reactor midplane (z = 0). The regions as modeled and starting from the inside ring are as follows (Fig. 20):

1. IFE inner sidewall
2. Inner unfueled region
3. Radial fueled region 1
   7.14–7.500 cm
4. Radial fueled region 2
   7.500–8.000 cm
5. Radial fueled region 3
   8.000–8.500 cm
6. Radial fueled region 4
   8.500–9.500 cm
7. Radial fueled region 5
   9.500–10.500 cm
8. Radial fueled region 6
   10.500–11.500 cm
9. Radial fueled region 7
   11.500–12.000 cm
10. Radial fueled region 8
    12.000–12.6 cm
11. Inner unfueled region
12. IFE outer sidewall
13. Water between IFE and the OFE

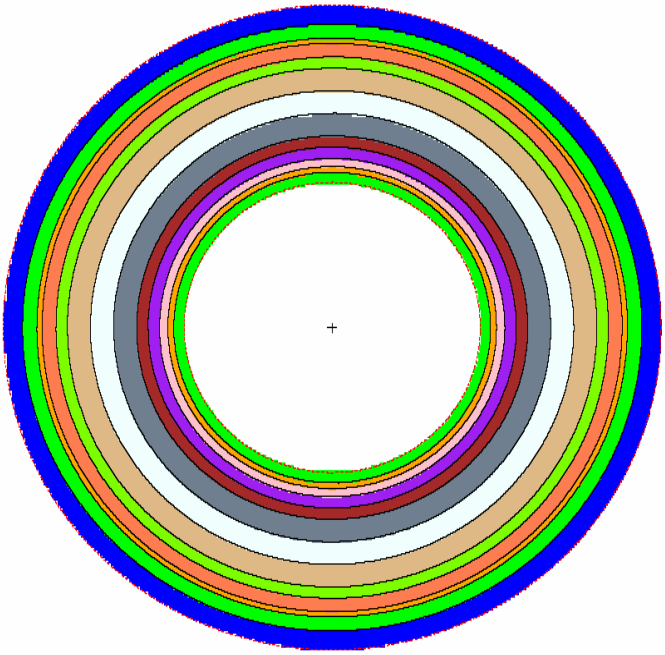

Fig. 20. Cross section of the IFE model x-y view at z = 0.

An axial profile of the model of the inner element is shown in Fig. 21. MCNP input corresponding to the inner fuel element is shown in Fig. 22.

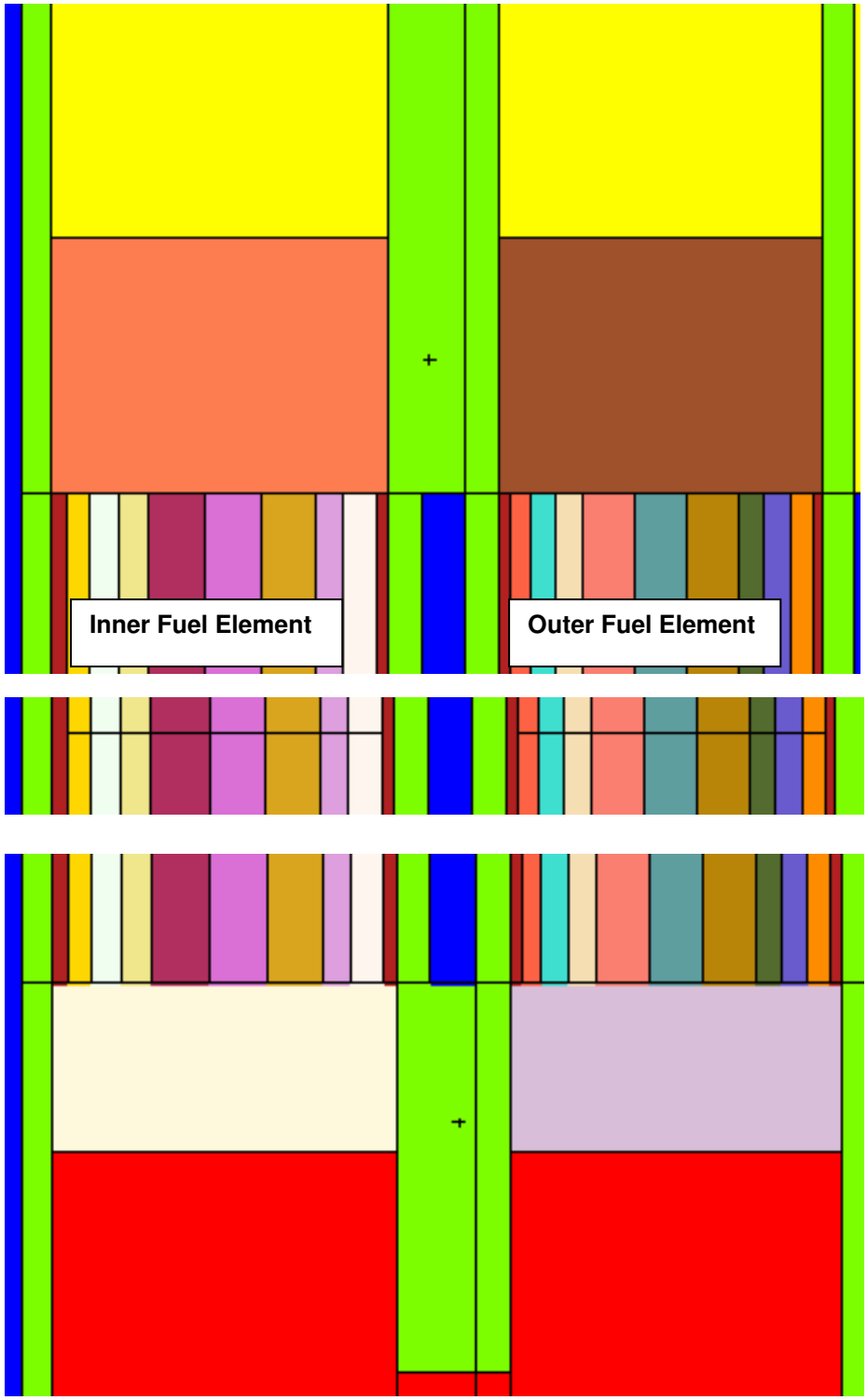

Fig. 21. x-z view of the fuel elements modeling.

```
c ************  Inner Fuel element Cell Cards  ****************
c
c
2000  20  6.02083-02   +1999  +200  -100 -2000  imp:n=1   $IFE inner sidewall
2100  200 8.01309-02   +2000  +200  -100 -2001  imp:n=1   $inner unfuelled region
c
c            ***** Coarse Zone Representation *****
c    Top -  Axial Layer 1  (25.4  - 19.0 cm)
2101  201 8.00804-02   +2001  +153  -100 -2002  imp:n=1   $ IFE radial fuelled region 1  7.14 - 7.5cm
2102  202 8.00839-02   +2002  +153  -100 -2003  imp:n=1   $ IFE radial fuelled region 2   7.5  - 8.0cm
2103  203 8.00880-02   +2003  +153  -100 -2004  imp:n=1   $ IFE radial fuelled region 3  8.0 - 8.50cm
2104  204 8.00937-02   +2004  +153  -100 -2005  imp:n=1   $ IFE radial fuelled region 4   8.5 - 9.5cm
2105  205 8.00993-02   +2005  +153  -100 -2006  imp:n=1   $ IFE radial fuelled region 5   9.5- 10.5cm
2106  206 8.00998-02   +2006  +153  -100 -2007  imp:n=1   $ IFE radial fuelled region 6  10.5-11.5cm
2107  207 8.00968-02   +2007  +153  -100 -2008  imp:n=1   $ IFE radial fuelled region 7  11.5 -12.cm
2108  208 8.00933-02   +2008  +153  -100 -2009  imp:n=1   $ IFE radial fuelled region 8  12.0-12.6cm
c
c
c        Inner fuel element--fuel regions
c       total atom density =  8.00804E-02 a/b-cm
m201  1001.66c  3.32434E-02  5010.66c   2.04121E-05   5011.66c  8.26896E-05
       8016.66c  1.71757E-02  12000.62c  1.33797E-04  13027.66c  2.89993E-02
      14000.60c  1.11291E-04 22000.62c  5.09408E-06  24000.50c  1.21958E-05
      25055.60c 6.57731E-06 26000.55c  4.14118E-05  29000.50c  2.77871E-05
      92234.66c  2.20708E-06  92235.66c  2.05700E-04  92236.66c  8.82838E-07
      92238.66c  1.19182E-05
mt201     lwtr.60t
c       total atom density =  8.00839E-02 a/b-cm
m202  1001.66c  3.32434E-02   5010.66c  1.77513E-05   5011.66c  7.19107E-05
       8016.66c  1.73053E-02  12000.62c  1.33797E-04  13027.66c  2.88388E-02
      14000.60c  1.10902E-04  22000.62c  5.09408E-06  24000.50c  1.21958E-05
      25055.60c  6.55746E-06 26000.55c   4.12166E-05  29000.50c  2.76915E-05
      92234.66c   2.69313E-06  92235.66c  2.51000E-04  92236.66c  1.07726E-06
      92238.66c  1.45429E-05
mt202     lwtr.60t
c       total atom density =  8.00880E-02 a/b-cm
m203  1001.66c  3.32434E-02   5010.66c  1.46911E-05   5011.66c  5.95138E-05
       8016.66c  1.74543E-02  12000.62c  1.33797E-04  13027.66c  2.86541E-02
      14000.60c  1.10456E-04  22000.62c  5.09408E-06  24000.50c  1.21958E-05
      25055.60c  6.53463E-06  26000.55c  4.09920E-05  29000.50c  2.75816E-05
      92234.66c  3.25214E-06  92235.66c  3.03100E-04  92236.66c  1.30087E-06
      92238.66c  1.75616E-05
mt203     lwtr.60t
c       total atom density =  8.00937E-02 a/b-cm
m204  1001.66c  3.32434E-02   5010.66c  1.03798E-05   5011.66c  4.20486E-05
       8016.66c  1.76644E-02  12000.62c  1.33797E-04  13027.66c  2.83940E-02
      14000.60c  1.09826E-04  22000.62c  5.09408E-06  24000.50c  1.21958E-05
      25055.60c  6.50246E-06  26000.55c  4.06755E-05  29000.50c  2.74266E-05
      92234.66c  4.03970E-06  92235.66c  3.76500E-04  92236.66c  1.61589E-06
      92238.66c  2.18144E-05
mt204     lwtr.60t
```

Fig. 22. MCNP input for IFE.

Fuel isotopic compositions for middle-of-cycle (MOC) and end-of-cycle (EOC) are also present in the HFV4.0 dataset. Material density cards for MOC and EOC are included in the model. The derivation of these atom densities are discussed in Refs. 4 through 9.

2.4 OUTER FUEL ELEMENT

The outer fuel element (OFE) consists of 369 fuel plates, each plate having an involute shape as shown in Fig. 23. Each plate contains 18.44 g ± 1% of ^{235}U. The OFE fueled area is modeled by dividing it into 63 cells, 9 radial fueled regions (Table 5), and 7 axial fueled layers. The nine radial regions represent the different effective ^{235}U concentrations (atoms per barn*cm) in the radial direction of the fuel plate (Figs. 24 and 25) at beginning-of-cycle. MCNP input corresponding to the outer element is shown in Fig. 26.

Fuel isotopic compositions for MOC and EOC are also present in the HFV4.0 dataset. Material density cards for MOC and EOC are included in the model. The derivation of these atom densities are discussed in Refs. 4 through 9.

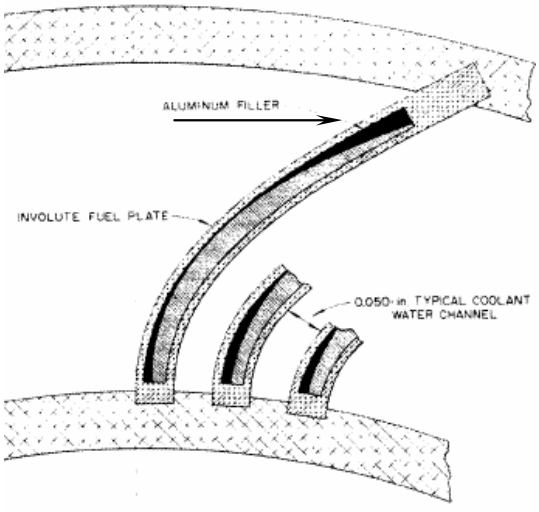

Fig. 23. Schematic of fuel plate configuration in OFE.

Table 5. Modeled regions in OFE

Radial fueled region number	Region thickness (cm)	^{235}U concentration [10^{-4} atoms/(bn*cm)]
1	15.1295–15.5	4.220
2	15.5–16.0	5.053
3	16.0–16.5	5.941
4	16.5–17.5	6.747
5	17.5–18.5	6.500
6	18.5–19.5	5.292
7	19.5–20.0	4.145
8	20.0–20.5	3.387
9	20.5–20.978	2.698

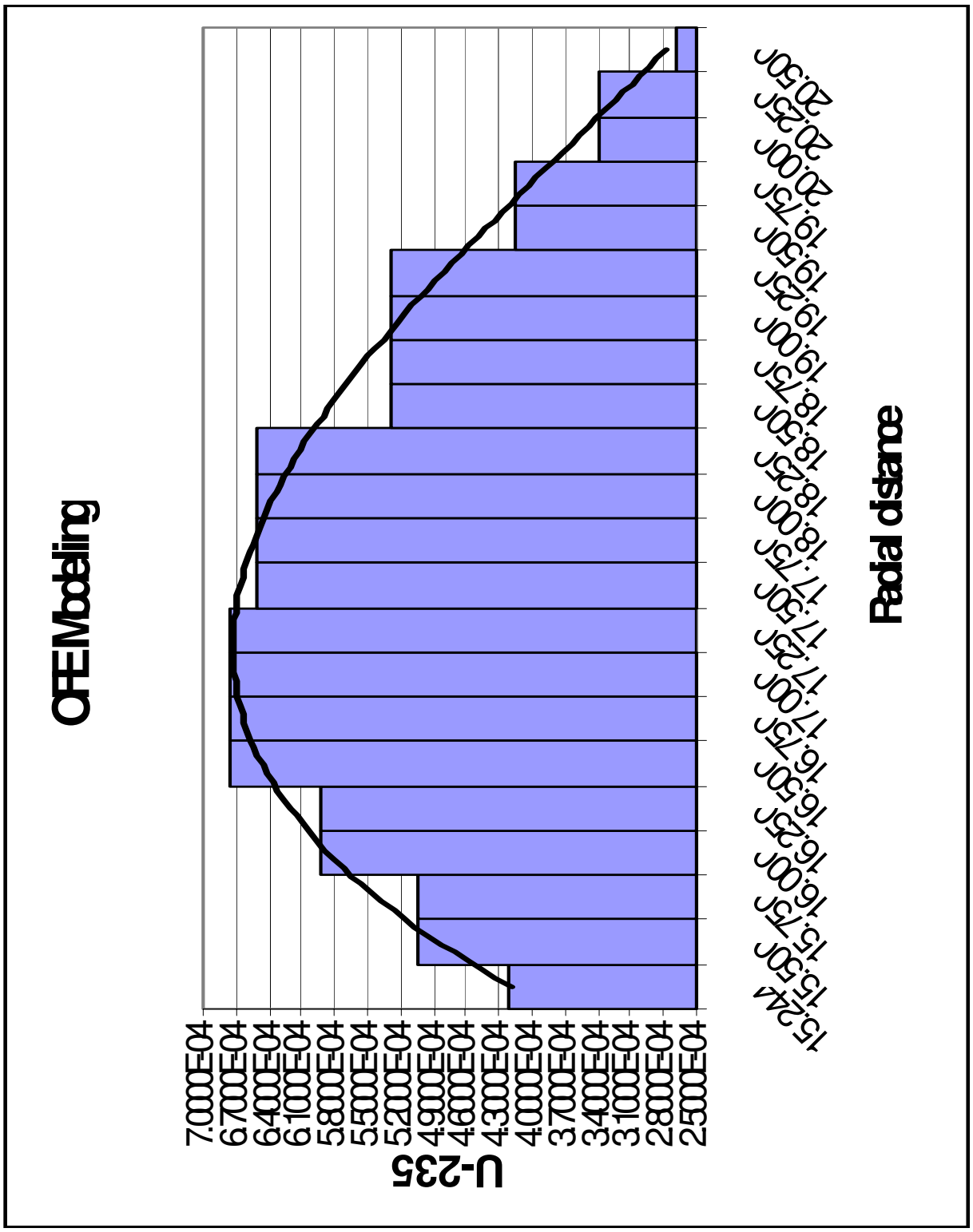

Fig. 24. Comparison of actual uranium distribution in outer element to modeled distribution.

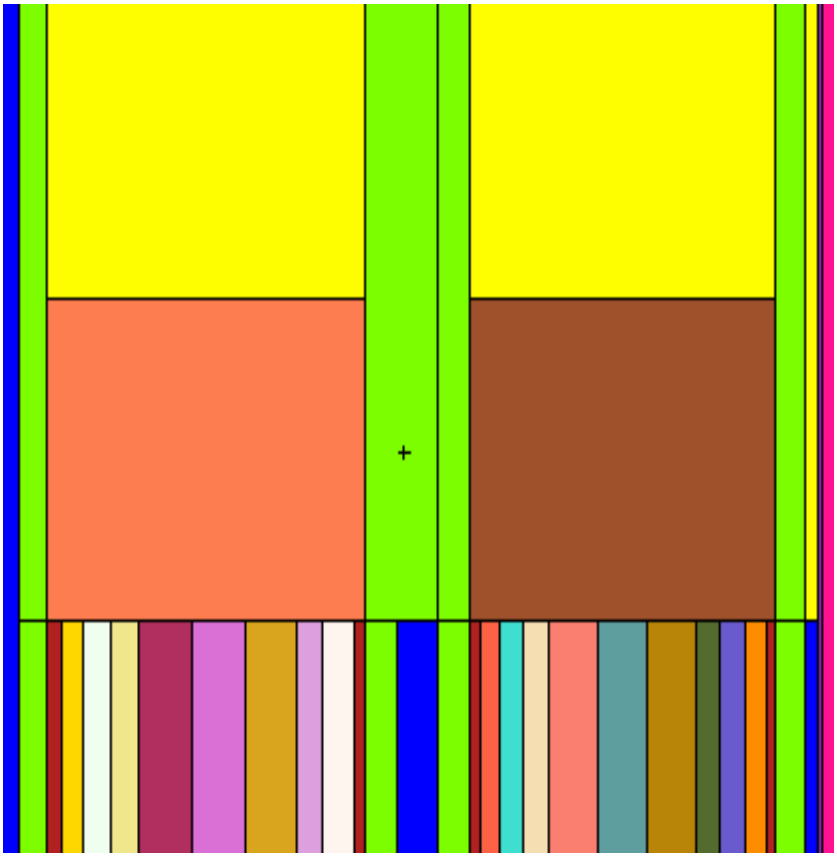

Fig. 25. Pictorial representation of MCNP model of fuel elements.

```
c ************ Outer Fuel element Cell Cards  ****************
c
2300  20  6.02083-02   +2201  +200  -100 -2300  imp:n=1   $OFE inner sidewall
2400  200 8.01309-02   +2300  +200  -100 -2301  imp:n=1   $outer unfuelled region
c
c             ***** Coarse Representation *****
c     Top - Axial  Layer 1    (25.4  - 19.0 cm)
2401  301 8.00583-02    +2301  +153  -100 -2302  imp:n=1   $  OFE radial fuelled region 1  15.1295 - 15.5 cm
2402  302 8.00895-02    +2302  +153  -100 -2303  imp:n=1   $ OFE radial fuelled region 2   15.5 - 16.0 cm
2403  303 8.01228-02    +2303  +153  -100 -2304  imp:n=1   $  OFE radial fuelled region 3   16.0 - 16.5 cm
2404  304 8.01530-02    +2304  +153  -100 -2305  imp:n=1   $  OFE radial fuelled region 4   16.5 - 17.5 cm
2405  305 8.01437-02    +2305  +153  -100 -2306  imp:n=1   $  OFE radial fuelled region 5   17.5 - 18.5 cm
2406  306 8.00985-02    +2306  +153  -100 -2307  imp:n=1   $  OFE radial fuelled region 6   18.5 - 19.5 cm
2407  307 8.00555-02    +2307  +153  -100 -2308  imp:n=1   $  OFE radial fuelled region 7   19.5 - 20.0 cm
2408  308 8.00271-02    +2308  +153  -100 -2309  imp:n=1   $  OFE radial fuelled region 8   20.0 - 20.5 cm
2409  309 8.00013-02    +2309  +153  -100 -2310  imp:n=1   $  OFE radial fuelled region 9   20.5 - 20.978 cm
c
c      *****Outer Fuel Element*****
c       total atom density =  8.00583E-02 a/b-cm
m301  1001.66c  3.32434E-02   8016.66c  1.77945E-02  12000.62c  1.33797E-04
13027.66c  2.82328E-02  14000.60c  1.09436E-04  22000.62c  5.09408E-06
24000.50c  1.21958E-05  25055.60c  6.48252E-06  26000.55c  4.04794E-05
29000.50c  2.73306E-05  92234.66c   4.52789E-06  92235.66c  4.22000E-04
92236.66c  1.81117E-06  92238.66c 2.44506E-05
mt301     lwtr.60t
c       total atom density =  8.00895E-02 a/b-cm
m302  1001.66c  3.32434E-02   8016.66c  1.80329E-02  12000.62c  1.33797E-04
13027.66c  2.79375E-02  14000.60c  1.08722E-04  22000.62c  5.09408E-06
24000.50c  1.21958E-05  25055.60c  6.44602E-06  26000.55c  4.01203E-05
29000.50c  2.71548E-05  92234.66c   5.42167E-06  92235.66c 5.05300E-04
92236.66c  2.16868E-06  92238.66c 2.92770E-05
mt302     lwtr.60t
c       total atom density =  8.01228E-02 a/b-cm
m303  1001.66c  3.32434E-02   8016.66c  1.82870E-02  12000.62c  1.33797E-04
13027.66c  2.76228E-02  14000.60c  1.07961E-04  22000.62c  5.09408E-06
24000.50c  1.21958E-05  25055.60c  6.40711E-06  26000.55c  3.97374E-05
29000.50c  2.69674E-05 92234.66c   6.37446E-06  92235.66c 5.94100E-04
92236.66c 2.54980E-06  92238.66c  3.44221E-05
mt303     lwtr.60t
c       total atom density =  8.01530E-02 a/b-cm
m304  1001.66c  3.32434E-02   8016.66c  1.85176E-02  12000.62c  1.33797E-04
13027.66c  2.73372E-02  14000.60c  1.07270E-04  22000.62c  5.09408E-06
24000.50c  1.21958E-05  25055.60c  6.37178E-06  26000.55c  3.93900E-05
29000.50c  2.67973E-05  92234.66c   7.23926E-06  92235.66c 6.74700E-04
92236.66c  2.89573E-06  92238.66c 3.90920E-05
```

Fig. 26. MCNP input corresponding to OFE.

```
mt304    lwtr.60t
c       total atom density =  8.01437E-02 a/b-cm
m305  1001.66c  3.32434E-02   8016.66c  1.84469E-02  12000.62c  1.33797E-04
      13027.66c  2.74247E-02  14000.60c  1.07482E-04  22000.62c  5.09408E-06
      24000.50c  1.21958E-05  25055.60c  6.38261E-06  26000.55c  3.94965E-05
      29000.50c  2.68494E-05  92234.66c   6.97424E-06  92235.66c  6.50000E-04
      92236.66c  2.78972E-06  92238.66c  3.76609E-05
mt305    lwtr.60t
c       total atom density =  8.00985E-02 a/b-cm
m306  1001.66c  3.32434E-02   8016.66c  1.81013E-02  12000.62c  1.33797E-04
      13027.66c  2.78528E-02  14000.60c  1.08517E-04  22000.62c  5.09408E-06
      24000.50c  1.21958E-05  25055.60c  6.43555E-06  26000.55c  4.00172E-05
      29000.50c  2.71044E-05  92234.66c  5.67811E-06  92235.66c  5.29200E-04
      92236.66c  2.27126E-06  92238.66c  3.06618E-05
mt306    lwtr.60t
c       total atom density =  8.00555E-02 a/b-cm
m307  1001.66c  3.32434E-02   8016.66c  1.77731E-02  12000.62c  1.33797E-04
      13027.66c  2.82593E-02  14000.60c  1.09501E-04  22000.62c  5.09408E-06
      24000.50c  1.21958E-05  25055.60c  6.48581E-06  26000.55c  4.05117E-05
      29000.50c  2.73464E-05  92234.66c   4.44742E-06  92235.66c  4.14500E-04
      92236.66c 1.77898E-06  92238.66c  2.40161E-05
mt307    lwtr.60t
c       total atom density =  8.00271E-02 a/b-cm
m308  1001.66c  3.32434E-02   8016.66c  1.75562E-02  12000.62c  1.33797E-04
      13027.66c  2.85280E-02  14000.60c  1.10150E-04  22000.62c  5.09408E-06
      24000.50c  1.21958E-05  25055.60c  6.51903E-06  26000.55c  4.08385E-05
      29000.50c  2.75064E-05  92234.66c   3.63412E-06  92235.66c  3.38700E-04
      92236.66c  1.45366E-06  92238.66c 1.96242E-05
mt308    lwtr.60t
c       total atom density =  8.00013E-02 a/b-cm
m309  1001.66c  3.32434E-02   8016.66c  1.73591E-02  12000.62c  1.33797E-04
      13027.66c  2.87722E-02  14000.60c  1.10741E-04  22000.62c  5.09408E-06
      24000.50c  1.21958E-05  25055.60c  6.54922E-06  26000.55c  4.11355E-05
      29000.50c  2.76518E-05 92234.66c  2.89485E-06  92235.66c  2.69800E-04
      92236.66c 1.15795E-06  92238.66c 1.56322E-05
mt309    lwtr.60t
c
```

Fig. 26. (continued).

2.5 CONTROL ELEMENTS

The control element region (CR) consists of two thin-walled (0.25-in.) concentric cylindrical zones. The inner cylindrical zone is, in reality, an annulus and is termed the lower or control cylinder or sometimes, the regulating element because its primary function is to regulate reactor power. That is, once a critical configuration has been established, slight vertical movements of the control cylinder are performed to adjust the level of reactor power. This rod moves upward to insert poison.

The outer concentric cylindrical zone is, in reality, divided into four quadrants, and each quadrant is termed a safety plate. Though each of the four plates has a separate drive mechanism, they are operated in tandem, and their position relative to the core axial midplane is symmetric to the control element. These four plates as a group are termed the safety element or, sometimes, the upper element.

Both the safety and regulating elements contain three longitudinal (axial) regions:

- black region containing europium (Eu_2O_3),
- gray region containing tantalum, and
- a white region containing aluminum.

All are clad with aluminum, making it an aluminum plate containing a black and gray cores (Fig. 27).

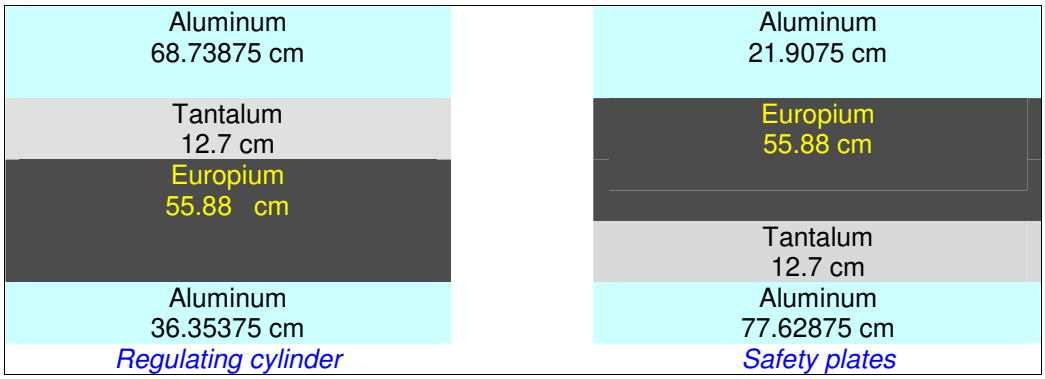

Fig. 27. Axial dimensions of regulating and safety elements.

The control element dimensions and height of each region are shown in Fig. 28. Gaps between four quadrants in the outer, safety element are explicitly modeled. The "flow holes" in the control elements are homogenized.

The model does not account for control element burnup, but this should have a minimal effect on the model (and on prediction of k_{eff}) because the control elements' worth generally does not change over the lifetime of the elements (nominally 100,000 MWd) and, in fact, increases slightly with use. This is due to the fact that europium absorbs neutrons and transmutes to gadolinium that has a higher neutron cross section than europium, and also that ^{181}Ta transmutes to ^{182}Ta under irradiation.

Control plates can be easily moved in the model by the use of surface transformation cards in order to set the plates at the corresponding position for the desired cycle time. Transformation cards corresponding to typical rod positions from HFIR operation used for beginning-of-cycle (BOC), EOC, and during cycle are included in the model and tabulated in Table 6. To run a particular case, one needs to use the transformation cards for that case, for both the inner and outer control plates instead of the ones used in the model (tr 87 and tr88) for BOC.

Cycle 400's balanced control rods measured positions as recorded by the reactor operators throughout the cycle operation are shown in Fig. 29 and in Table 7. The data plotted in Fig. 29 are available from the reactor operator's log for cycle 400. Perturbations in the otherwise "smooth" withdrawal of safety plates are presumed to be due to rebalancing the control and safety plates, that is, ensuring that control and safety element positions are maintained as symmetric to core centerline. During cycle 400, the reactor operated for a total of 592 h, during which time the control elements were withdrawn from 18.0 in. at BOC, to 26.86 in. at EOC, resulting in a net withdrawal of 8.86 in. for the entire cycle.

That portion of the MCNP file corresponding to the control element zone is shown in Fig. 30. Visualization of that input is shown in Fig. 31.

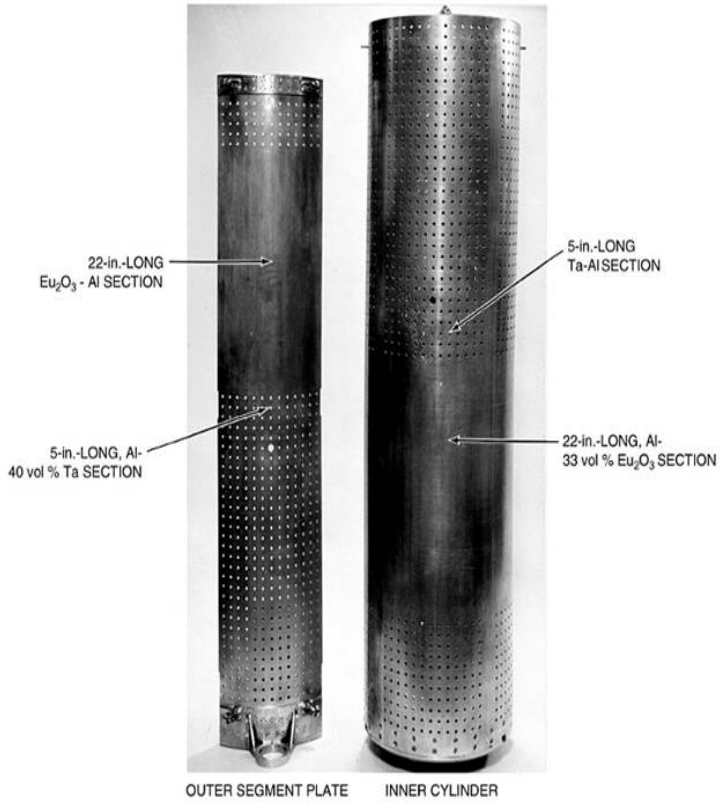

Fig. 28. Picture of safety and regulating elements.

Table 6. Control rod positions in MCNP model (inner moves down, outer moves up)

Case/Comment	Time in cycle (d)	Position (in. withdrawn)	Model Position (cm)	Inner Tr card	Outer Tr card
Shutdown Black regions at upper/lower edge of unfueled core region	0.0	0.0	0.000	83	84
Control elements fully inserted; Black regions at upper/lower edge of active region	0.0	2.0	5.080	85	86
Startup	0.0	18.0	45.720	87	88
Xenon at equilibrium	1.0	19.25	48.895	89	90
Depletion steps; Fission products simulated by boron and a lumped fission product	2.0	20.25	51.435	91	92
	10.0	21.0	53.340	93	94
	18.0	23.50	59.690	95	96
	20.0	25.00	63.500	97	98
EOC White regions at upper/lower edge of active region)	24.3	27.0	68.580	101	102

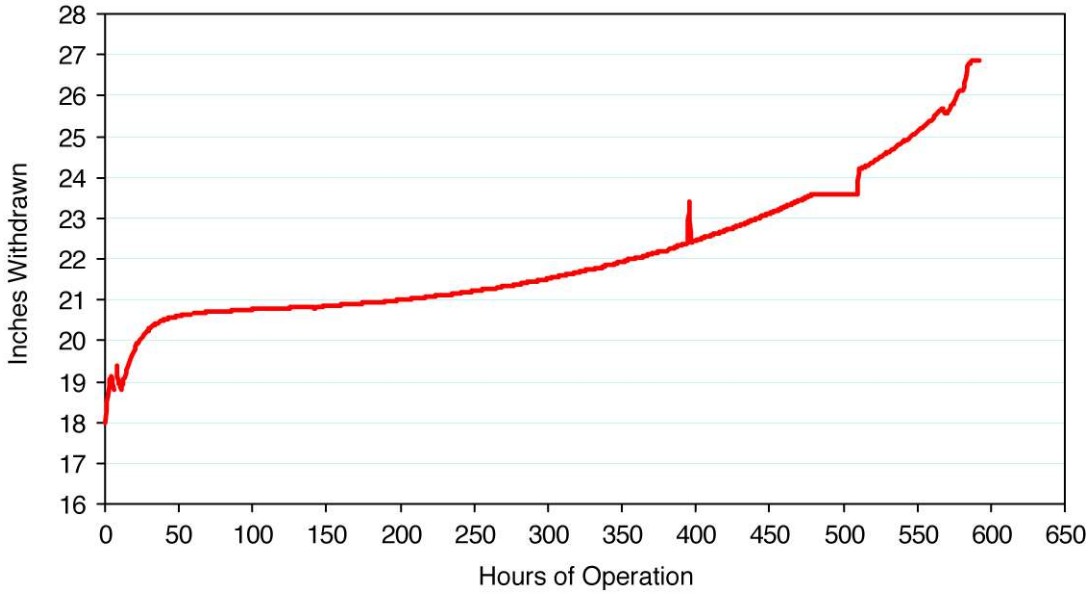

Fig. 29. Cycle 400 balanced rod position (control elements 1–4).

Table 7. Safety plates (control elements 1–4) position for cycle 400

Time (d)	Safety plates position (inches withdrawn)	Time (d)	Safety plates position (inches withdrawn)
0.000	18.00	11	21.28
0.042	18.33	12	21.44
0.083	18.64	13	21.61
0.500	18.97	14	21.78
0.625	19.34	15	22.02
1	20.05	16	22.27
2	20.43	17	22.54
3	20.66	18	22.85
4	20.72	19	23.19
5	20.77	20	23.59
6	20.82	21	23.59
7	20.87	22	24.56
8	20.93	23	25.19
9	21.01	24	25.90
10	21.17	24.67[a]	26.86

[a]Shutdown, exposure = 2068.42 MWd.

```
c     ************  Control Element Cell Cards   ******************
c
3000  2   9.95227-02    +2400  +200  -100 -3000  imp:n=1 $water btw OFE and inner CR-active region
3001  3   1.00053-01    +2400  -199  +100 -3000  imp:n=1 $wter btw OFE & inner CR--above active rgn
3002  1   9.89921-02    +2400  +299  -200 -3000  imp:n=1 $wter btw OFE & inner CR--below active rgn
c
c      Inner control element
c
3100  3     1.00053-01    +3000  +300  -199 -3003  imp:n=1   $Inner element--Upper H2O
3101  1     9.89921-02    +3000  +299  -304 -3003  imp:n=1   $Inner element--Lower H2O
c
3110  21    6.02083-02    +3000  +304  -300 -3001  imp:n=1   $Inner element--Inner clad
3111  402    6.21902-02     +3001  +301  -300 -3002  imp:n=1   $Inner element--Upper white region
c
3112   21    6.02083-02    -700  +701 +3001  +303  -301 -3002  imp:n=1   $Inner element-Al gap region
1
3113   21    6.02083-02     703  -702 +3001  +303  -301 -3002  imp:n=1   $Inner element-Al gap region 2
c
3114  400   6.02937-02    +700  +702 +3001  +302  -301 -3002  imp:n=1   $Inner element--Gray -Quad
1
3115  401   6.13221-02    +700  +702 +3001  +303  -302 -3002  imp:n=1   $Inner element-Black -Quad
1
3116  400   6.02937-02     -703  +700 +3001  +302  -301 -3002  imp:n=1   $Inner element--Gray -Quad
2
3117  401   6.13221-02     -703  +700 +3001  +303  -302 -3002  imp:n=1   $Inner element-Black-Quad 2
3118  400   6.02937-02     -701  -703 +3001  +302  -301 -3002  imp:n=1   $Inner element--Gray -Quad 3
3119  401   6.13221-02    -701  -703 +3001  +303  -302 -3002  imp:n=1   $Inner element--Black -Quad 3
3120  400   6.02937-02      702  -701 +3001  +302  -301 -3002  imp:n=1   $Inner element--Gray-Quad 4
3121  401   6.13221-02      702  -701 +3001  +303  -302 -3002  imp:n=1   $Inner element--Black-Quad 4
c
3122  403    6.21521-02     +3001  +304  -303 -3002  imp:n=1   $Inner element--Lower white region
3123  21    6.02083-02    +3002  +304  -300 -3003  imp:n=1   $Inner element--Outer clad
c
c      Water btw control elements
3200  2   9.95227-02  +3003  +200  -100 -3004  imp:n=1 $wtr btw inner CR and outer CR--active region
3201  3   1.00053-01  +3003  -199  +100 -3004  imp:n=1 $wtr btw inner  and outer CR--above active rgn
3202  1   9.89921-02  +3003  +299  -200 -3004  imp:n=1 $wtr btw inner and outer CR--below active rgn
C
 c         ***** Control Rod Positions ***** (inner moves down outer moves up)
c Surface transformations used to set the control plates position in the model -2 tr. used for each position
c    inner tr.    outer tr.
c     83    and     84       ** SHUTDOWN - 0.0 inch - shutdown (black rgns at edge of unfuelled core rgn)
c     85    and     86       ** FULLY INSERTED - 2.0 inch - startup (black rgns at  edge of active region)
c     87    and     88        ***** STARTUP - 18.0 inch - 0.0 days
c     89    and     90       ***** Xe - 19.25 inch - 1.0 days
c     91    and     92        ***** Boron Burn - 20.25 inch - 2.0 days
c     93    and     94        *****  - 21.00 inch - 10.0 days
c     95    and     96         *****  - 23.50 inch - 18.0 days
c     97    and     98         *****  - 25.00 inch - 20.0 days
c     99    and    100        ***** AVERAGE POSITION - 22.0 inch - 14.0 days
c    101 and     102        ***** FULLY WITHDRAWN - 27.0 inch
```

Fig. 30. MCNP input corresponding to regulating and safety elements.

```
c
c Material  for control elements
c
c       Aluminum clad of control elements
m21      13027.66c   5.85482-02  1001.66c    3.45716-04 12000.62c    6.68986-04
        14000.60c   3.47363-04 22000.62c    2.54704-05 24000.50c    6.09789-05
        25055.60c   2.21974-05 26000.55c    1.01905-04 29000.50c    8.74557-05
c
c
c      *****Inner Control Element*****
c       Inner control element--Gray Ta-Al/H2O region
m400     73181.66c  2.10142-02 13027.66c    3.43728-02   1001.66c   3.27118-03
           8016.66c  1.63559-03
mt400    lwtr.60t
c       Inner control element--black EuO-Al region
m401     63151.66c  4.04205-03 63153.66c    4.41415-03  13027.66c   4.01816-02
           8016.66c  1.26843-02
c       Inner control element-upper Al/H2O region
m402       1001.66c  3.26363-03  8016.66c    1.63181-03  13027.66c   5.72947-02
mt402      lwtr.60t
c       Inner control element-lower Al/H2O region
m403       1001.66c  3.19976-03  8016.66c    1.59988-03  13027.66c   5.73524-02
mt403    lwtr.60t
c
c
c      *****Outer Control Element*****
c       Outer control element--Gray Ta-Al/H2O region
m411     73181.66c  2.10212-02  13027.66c   3.43843-02   1001.66c   3.24993-03
           8016.66c   1.62497-03
mt411    lwtr.60t
c       Outer control element--black EuO-Al region
m410     63151.66c   4.04205-03  63153.66c   4.41415-03  13027.66c   4.01816-02
           8016.66c   1.26843-02
c       Outer control element-upper Al/H2O region
m412       1001.66c  3.01443-03  8016.66c    1.50722-03  13027.66c   5.75198-02
mt412    lwtr.60t
c       Outer control element-lower Al/H2O region
m413       1001.66c  3.19012-03  8016.66c    1.59506-03  13027.66c   5.73611-02
mt413    lwtr.60t
c
```

Fig. 30. (continued)

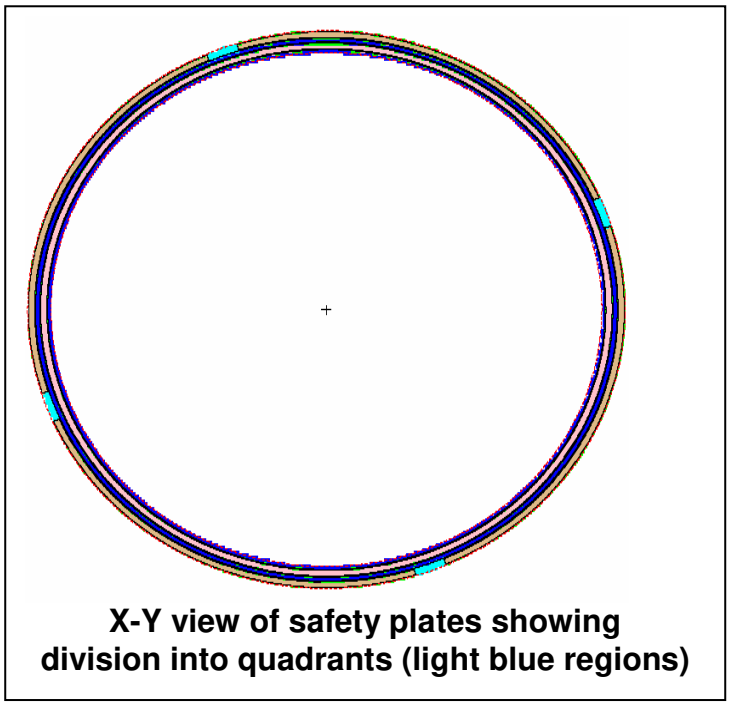

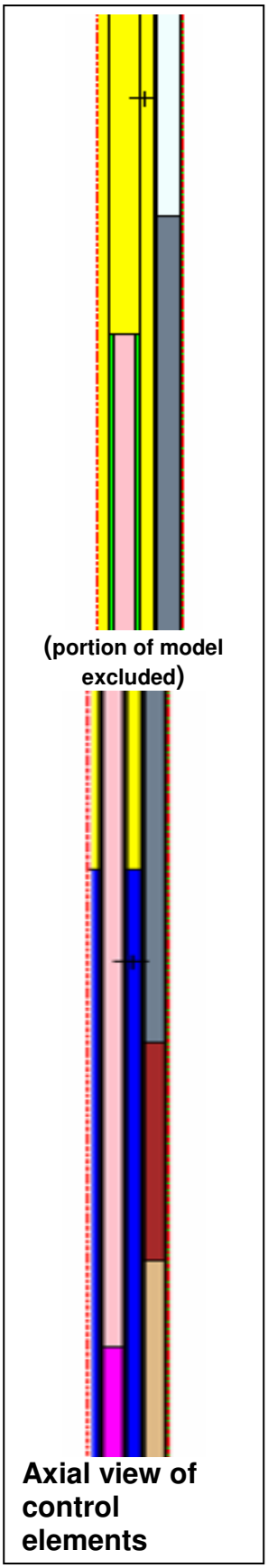

Fig. 31. Visualization of MCNP model for control element zone.

2.6 REMOVABLE AND SEMIPERMANENT REFLECTORS

Due to embrittlement caused by radiation, the inner 5 cm (2 in.) of the beryllium reflector must be replaced after 40 cycles of operation of the reactor. At the start of cycle 400, a new removable beryllium reflector was placed in the reactor.

The semipermanent reflector—that portion containing the control rod access plugs—is replaced every 80 cycles. The composition of the beryllium in all the reflectors is the same however the presence of cooling water channels causes homogenized atom densities for the three reflector regions to differ.

Twenty experiment facilities are located in this region and include:

- eight large RB positions designated in pairs, e.g., RB1 and RB1*, located in the removable beryllium zone,
- four small RB positions located in the semipermanent beryllium reflector and,
- eight control-rod (CR) access plug facilities located in the semipermanent beryllium reflector.

Large RB positions are explicitly modeled with an aluminum liner. That portion of the MCNP input file that represents the material for the removable and semipermanent reflectors is shown in Fig. 32. Visualization of this input is shown in Fig. 33.

```
c     Beryllium removable reflector
c       At the start of cycle 400, a new removable beryllium reflector was placed in the reactor
c       No Li-6, or He-3 present (100% Be - H2O gaps are explicitly modeled)
c
m101     4009.66c  1.23607-01    $ Removable reflector Rgn 1 material
mt101    be.60t
m102     4009.66c  1.23607-01    $ Removable reflector Rgn 2 material
mt102    be.60t
m103     4009.66c  1.23607-01    $ Removable reflector Rgn 3 material
mt103    be.60t
m104     4009.66c 1.23607-01  3006.66c 3.14456-7  2003.66c 9.25940-9   $semi-permanent refl. reg
mt104    be.60t
c
c
```

Fig. 32. MCNP input for removable and semipermanent reflector.

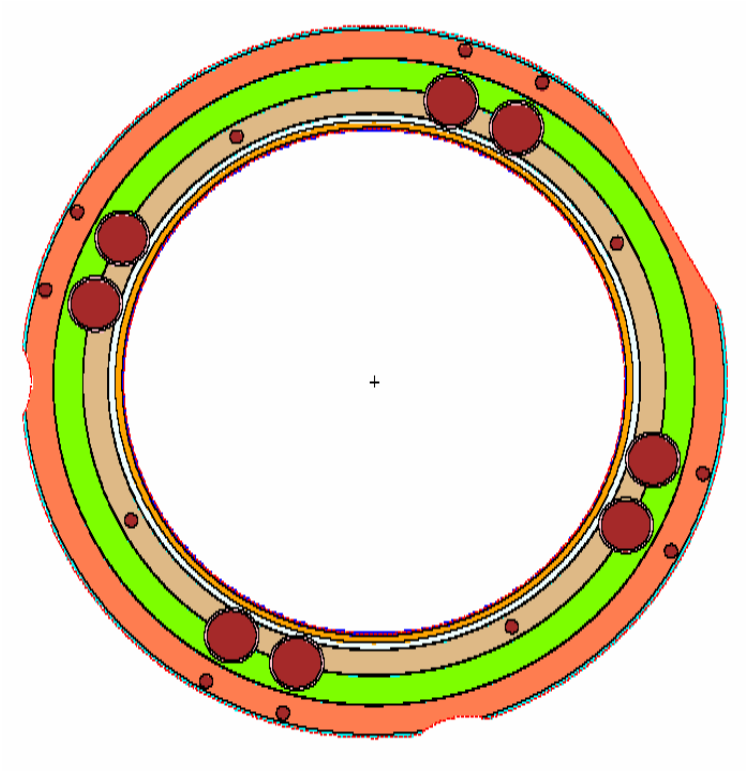

Fig. 33. Representation of MCNP model of removable and semipermanent reflector.

2.7 THE PERMANENT BERYLLIUM REFLECTOR, WATER SHIELD, AND PRESSURE VESSEL

The permanent beryllium reflector extends approximately 20 cm beyond the outside radius of the semipermanent reflector. It is surrounded by approximately 50 cm of water and then the steel pressure vessel. The permanent beryllium reflector is replaced every 135 cycles. The permanent reflector is shown in Fig. 34 and includes

- large VXF—6;
- inner small VXF—11;
- outer small VXF—5;
- engineering facilities (vertical slant tubes) –2 existing, 4 modeled;
- HB-1/HB-4 though tube;
- HB-2 radial beam tube; and
- HB-3 tangential beam tube.

The reflector as modeled is shown in Fig. 35. The VXF positions are modeled with stainless steel liners. Equilibrium poisons (Li-6 and He-3) resulting from fast neutron reactions in beryllium are modeled in a zone-wise fashion in the reflector. Atom densities and zone boundaries are given in Table 8.

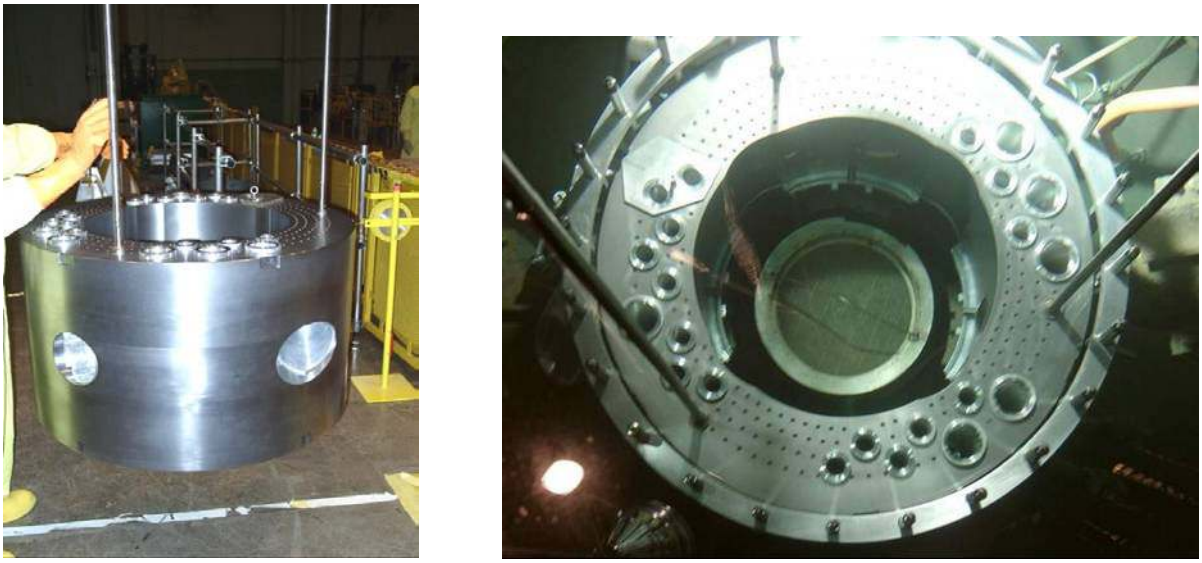

Fig. 34. Views of the permanent beryllium reflector.

Table 8. Neutron poisons modeled in permanent beryllium reflector

Inner radius of zone (cm)	Material No.	Lithium-6 atom density [atoms/(bn*cm)]	Helium-3 atom density [atoms/(bn*cm)]
33.3375	105	$1.74120(10^{-7})$	$5.11969(10^{-9})$
36.3375	106	$1.08525(10^{-7})$	$4.29666(10^{-9})$
39.3375	107	$7.10578(10^{-8})$	$2.07747(10^{-9})$
42.3375	108	$4.80664(10^{-8})$	$1.39911(10^{-9})$
45.3375	109	$3.32031(10^{-8})$	$9.59631(10^{-10})$
48.3375	110	$2.46752(10^{-8})$	$7.06338(10^{-10})$
51.3375	111	$1.84489(10^{-8})$	$5.19306(10^{-10})$

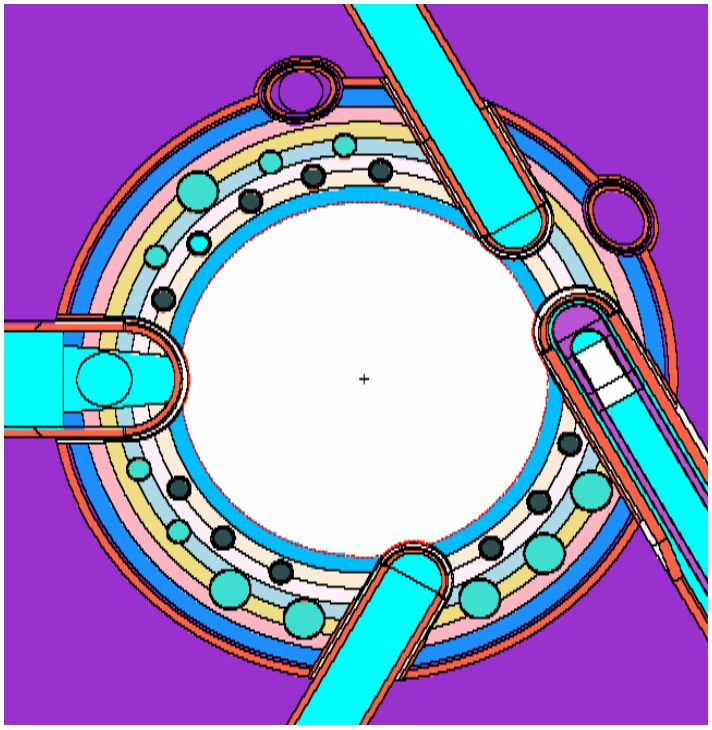

Fig. 35. MCNP model of the permanent beryllium reflector region, showing 22 VXF, 4 experimental facilities, and the HB tubes.

The HFIR was constructed with four engineering facilities (slant tubes) as shown in Fig. 3. Two of these were eliminated during the enlargement of the HB-2 beam tube leading to the current configuration that is shown in Fig. 4. The MCNP model documented in Ref. 4 contains the current permanent beryllium configuration as shown in Fig. 4.

3. RESULTS OF CALCULATIONS

3.1 SENSITIVITY OF MULTIPLICATION FACTOR TO MODEL ASSUMPTIONS

Several calculations were performed to arrive at the best model that most accurately simulates the HFIR. Several cross section datasets were examined, and variations in number of cycle histories were considered. A summary of the results is shown in Table 9.

Table 9. MCNP calculation of the HFIR at BOC

MCNP model	Number of histories	Number of neutrons per cycle	Cross section library	Final k-effective (col/abs/trk len)	SD standard deviation
V44	50,000,000	1000	rmccs	1.00504	0.00019
V49	50,000,000	1000	endf/B-VI	1.00789	0.00013
V56	60,000,000	2000	endf-.66c	1.00834	0.00012
V58	60,000,000	2000	endf .61c	1.01235	0.00012
V57	60,235,653	600	endf-.66c	1.00830	0.00012
V29a	60,125,000	1000	endf6-.66c	1.00884	0.00012
V29b	60,125,000	1000	endf5-.50c	1.00681	0.00012

The difference between the V44 and V49 models is the use of the endf66 cross section library; the V44 case was executed with a somewhat older data library, rmccs (recommended Monte Carlo cross section library). The increase in k_{eff} between the two cases is significant and was not expected because cross section data have not changed significantly in recent years especially for known, common nuclear reactor elements like uranium, water, and aluminum. One reason for this increase may be the presence of delayed neutron data. The rmccs data for uranium isotopes (92234.50c, 92235.50c, 92238.50c) all lack delayed neutron data. Data in endf66 include the delayed neutron contribution for these uranium isotopes (92234.66c, 92235.66c, 92238.66).

In the V56 run, the number of neutrons per cycle was increased from the V49 case. The number of histories was comparable, and while the value of k increased slightly, the change was not statistically significant.

In run V58, two changes were made from case V56—the first using a different, and older cross section dataset for uranium, endf.61c, and second, the assignment of cross section data to the water between the fuel elements was changed to ltw.01t, which allows for use of "S-alpha-beta" data for scattering. Although this assignment had been made for the rest of the reactor, it was missed in the older models and in earlier models. These changes had a significant effect on the multiplication factor.

Case V57 was calculated using endf.66 data; the most recent data were available with the ^{235}U dataset containing a larger number of measured values than in the other libraries. Additionally, the aluminum in the solid target rods was changed from pure aluminum to the actual alloy, Al-1100. Calculations were run for 600 neutrons/cycle for 100,000 cycles, resulting in 60 million histories.

Cases 29 a and b were performed with all the actual cycle 400 PTP experimental loading in the model.

3.2 BOC CALCULATIONS

The final model for BOC MCNP Monte Carlo calculations was designated the HFV4.0 model. The BOC conditions include 9.4 kg of ^{235}U, 2.8 g of boron (^{10}B) in the IFE, and with the control rods at 18-in. position. The model was case V57 but with ltw.06t cross section data used for all water regions and graph.06 used for graphite material in the target region. The calculated eigenvalue (k_{eff}) was 1.0083 ± 0.00012; Figs. 36–38 show the calculated eigenvalue for k absorption, k-collision, and k track.

The model does accurately predict the multiplication factor for the reactor to within 1%. We think that this value could be used with confidence as a base number to calculate the reactivity change of loading new experiments to the core, for both safety and neutronics calculations.

The less than 1% overestimation of k_{eff} for the HFV4.0 model could be due to many reasons. The most obvious is experimental and target loading. The atom densities and descriptions of some experimental loadings were not available; thus, the sites were left empty in our calculations. Including all the experimental loadings in the model will decrease the value of k_{eff} by a small amount, but we do not think that it will bring it to 1.0000.

A few other assumptions were made in the modeling, and many regions were homogenized. The exact atom density of many materials and the presence of trace elements does effect neutrons and thus k.

Cross section data are not perfect, and as we have shown throughout this report, the results of eigenvalues calculations will vary depending on which library is used. These data are being continuously updated, and thus updating cross sections will continue to improve the model.

The HFV4.0 model is based on the most recent continuous energy neutron cross section data from several libraries. The available data are evaluated at 293.6°K. The HFIR fuel plate centerline temperature is 435°K, and the metal-oxide interface temperature is 423°K.

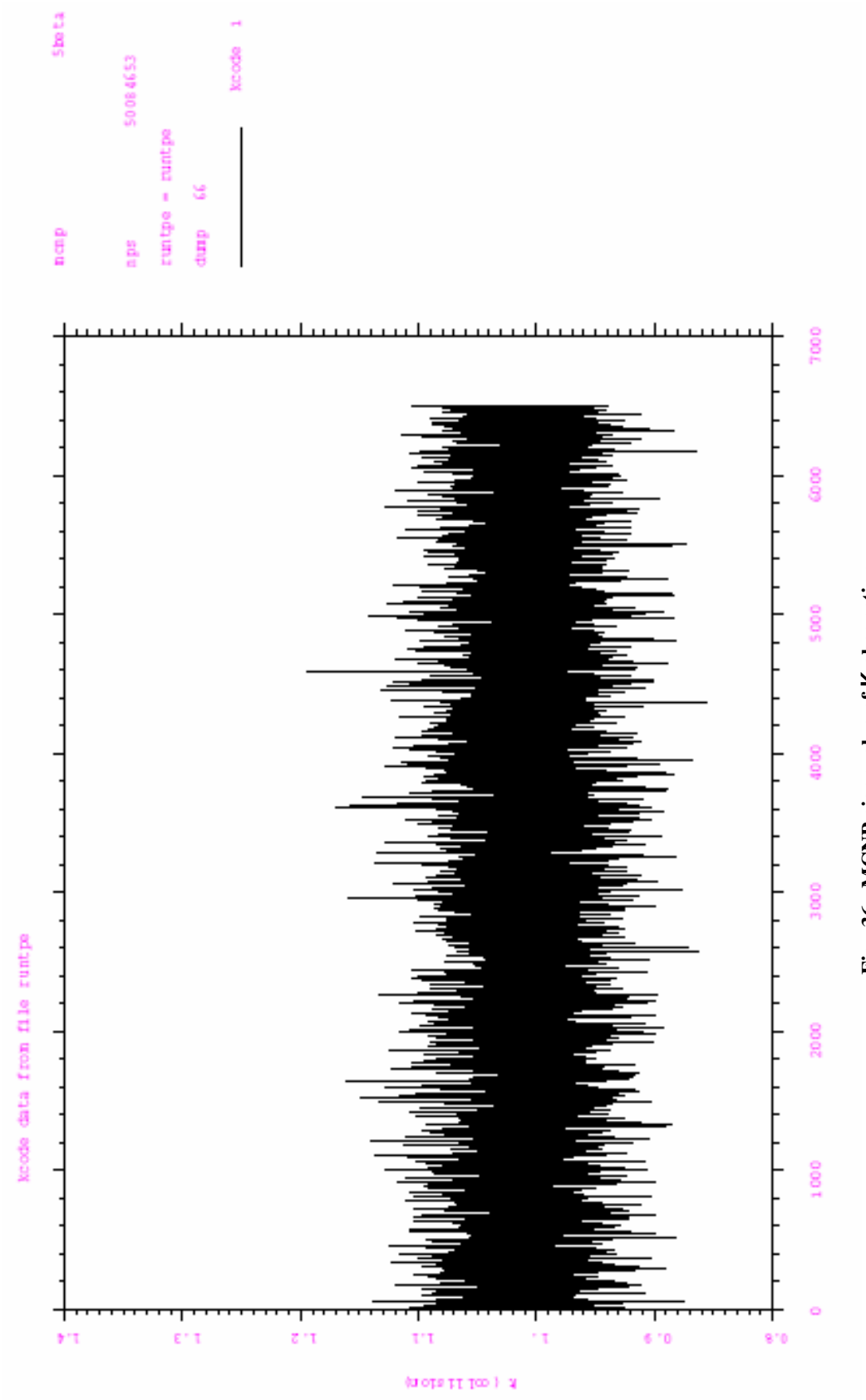

Fig. 36. MCNP eigenvalue of K absorption.

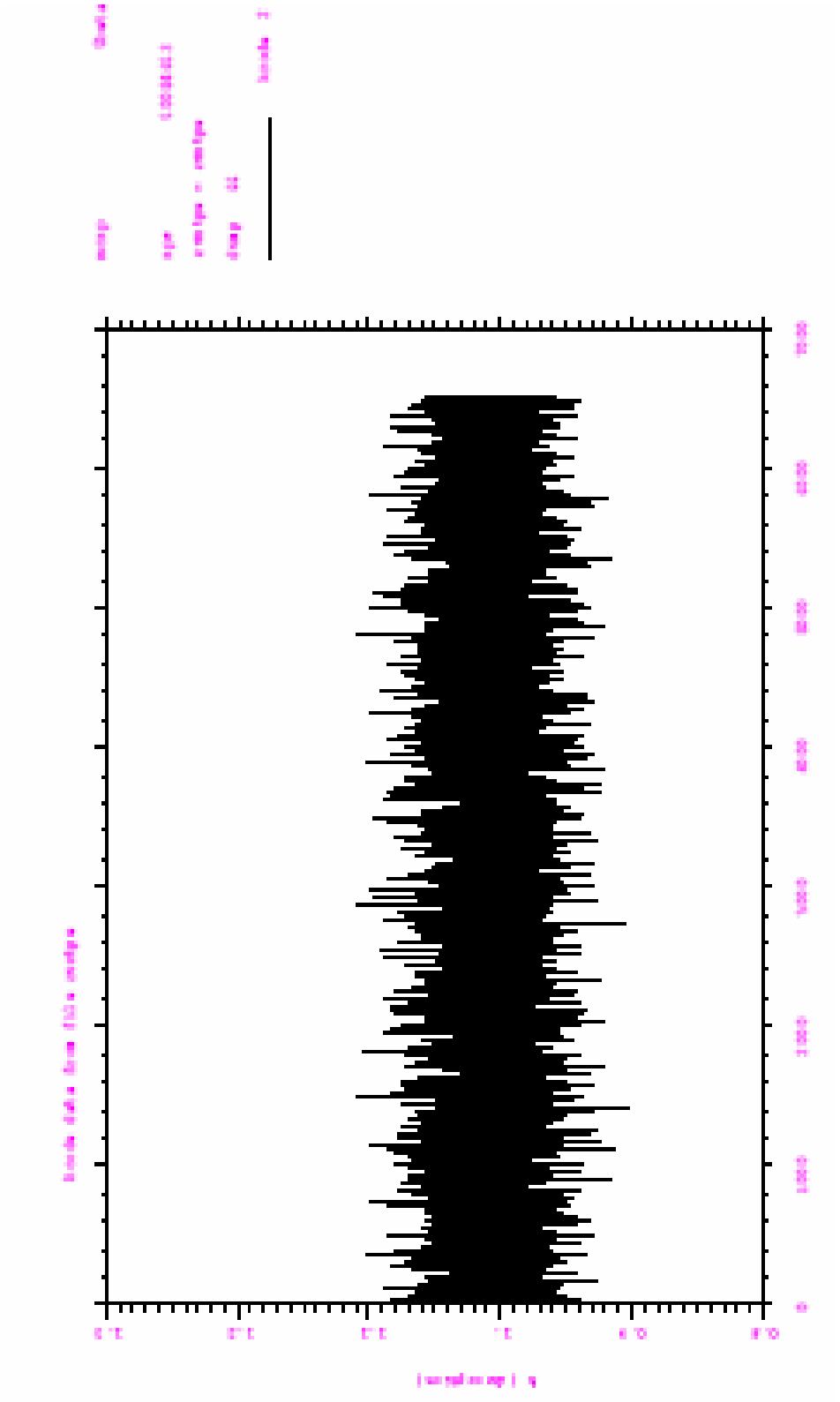

Fig. 37. MCNP eigenvalue of K collision.

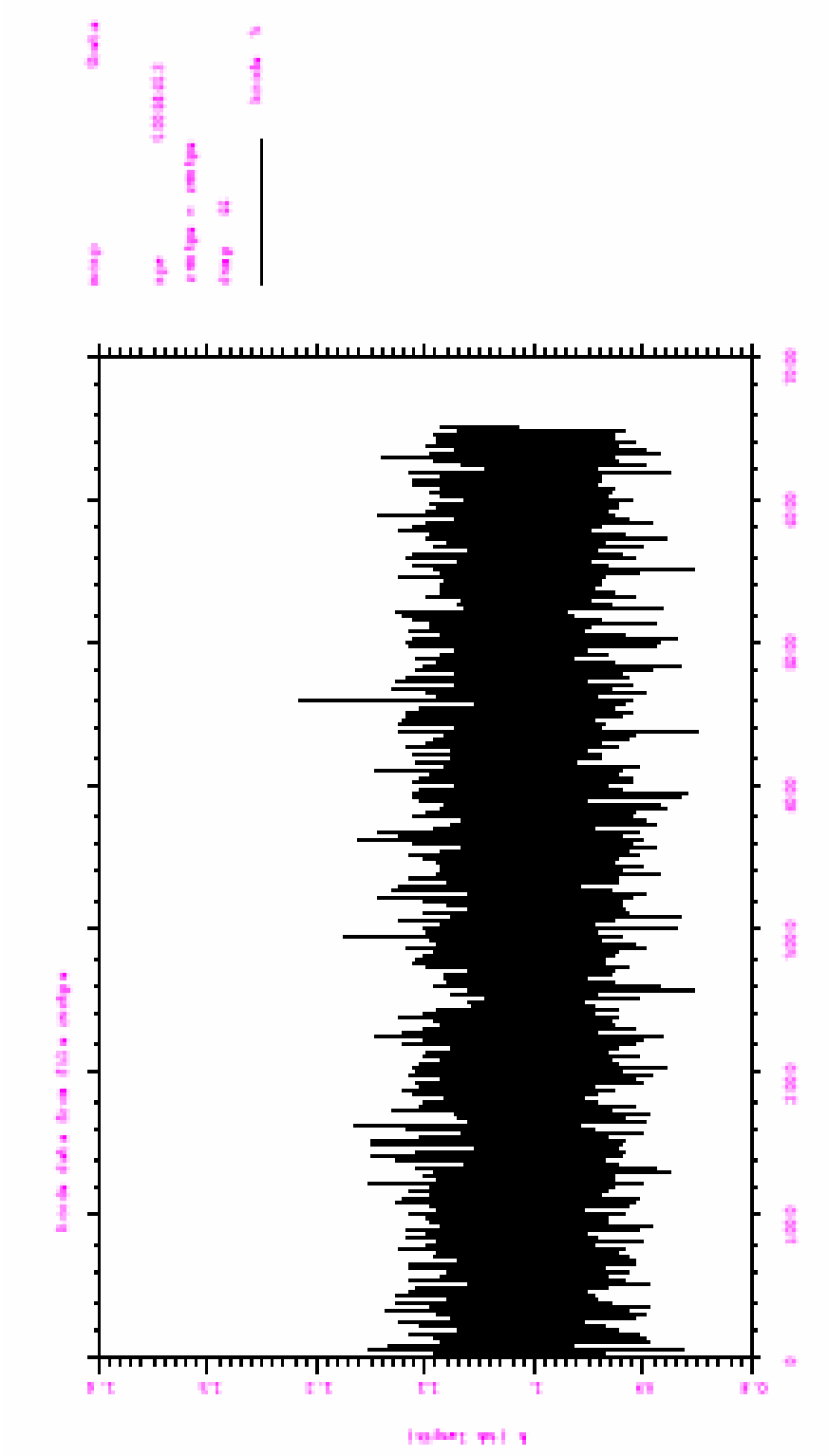

Fig. 38. MCNP eigenvalue of K track.

This increase in the temperature of the fuel results in Doppler broadening of resonances and a change in the neutron absorption cross section. The cross sections used in this model are processed by NJOY and already include Doppler broadening of elastic, capture, fission, and other low-threshold absorption cross-sections (<1 eV). Thus, temperature cards should not have any noticeable effect on MCNP calculations using this model.

3.3 REACTOR PARAMETERS CALCULATIONS

The HFV4.0 model can be used to estimate various important reactor parameters. Neutron flux, fission rate, neutron gamma, and other reaction rates can all be tallied using this MCNP model.

To obtain the absolute values, tallies from MCNP calculations must be normalized to the HFIR source by multiplying the tallies by the total source of neutrons for the HFIR operating at 85 MW, or by multiplying by the source per watt power. The HFIR source is calculated as follows:

$$\textit{Total source} = (2.43 \text{ neutrons/fission}) * (85 \times 10^{6} \text{ W})/[(200.7 \text{ MeV/fission}) (1.602177 \times 10^{-13} \text{ J/MeV})] = 6.4234 \times 10^{18} \text{ neutrons/s}$$

$$\textit{Source/watt power} = (2.43 \text{ neutrons/fission})/[(200.7 \text{ MeV/fission}) (1.602177 \times 10^{-13} \text{ J/MeV})] = 7.56 \times 10^{10} \text{ neutrons/s-W}$$

3.3.1 Neutron Fluxes

The neutron fluxes in the flux trap region were calculated for cycle 400 and compared with values reported by Cheverton and Sims. The thermal (0–0.414 eV) and total neutron fluxes are presented in Fig. 39 and Fig. 40. The flux was tallied at the reactor midplane, where it is known to have the highest magnitude, over a very small height of –0.1 and +0.1 cm around the reactor midplane. The absolute neutron flux values were obtained by multiplying the tallies by the HFIR true source strength per megawatt of power.

3.3.2 Neutron/Gamma Heat Generation

Neutron gamma reactions in several locations in the flux trap region were tallied using the model. The heat generation caused by neutron interactions in those cells that are loaded with solid aluminum dummy targets was calculated using the MCNP model HFV4.0. Values are presented in Table 10. It is important to note that for aluminum structures, the ^{28}Al beta decay and associated gamma ray production contribute considerably more energy deposition than that of direct neutron heating.

Table 10. Neutron heat generation rate in solid aluminum targets

Cell No.	Tally	J/MeV	Source	W/g
490	3.82E-07	1.60E-13	6.42E+18	0.394
530	3.82E-07	1.60E-13	6.42E+18	0.394
560	3.69E-07	1.60E-13	6.42E+18	0.379
579	7.38E-07	1.60E-13	6.42E+18	0.760
649	7.58E-07	1.60E-13	6.42E+18	0.780
650	3.81E-07	1.60E-13	6.42E+18	0.392
690	3.78E-07	1.60E-13	6.42E+18	0.389
Average				0.498

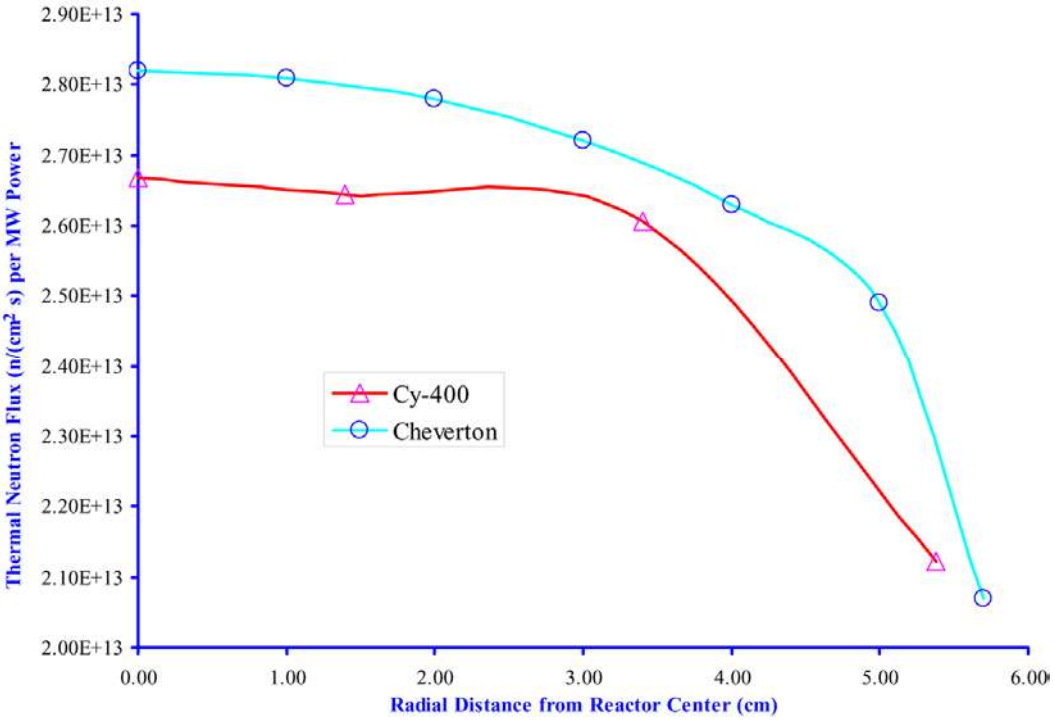

Fig. 39. Thermal neutron flux [n/(cm^2*s)].

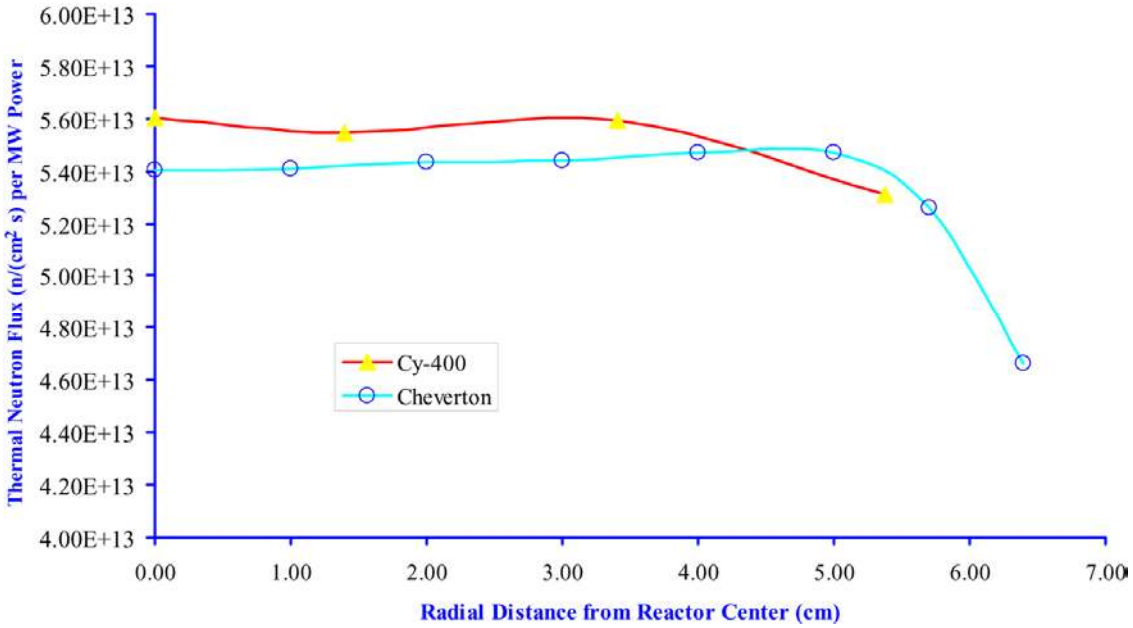

Fig. 40. Total neutron flux [n/(cm^2*s)].

3.3.3 Fission Rate Density

The fission rates at the reactor midplane were calculated in the IFE and the OFE. The absolute fission rates in the fuel elements were obtained by multiplying the MCNP tallies with HFIR total source of the reactor at 85 MW power, which is equal to 6.4234×10^{18} neutrons/s. The fission rates at the reactor midplane are shown in Fig. 41.

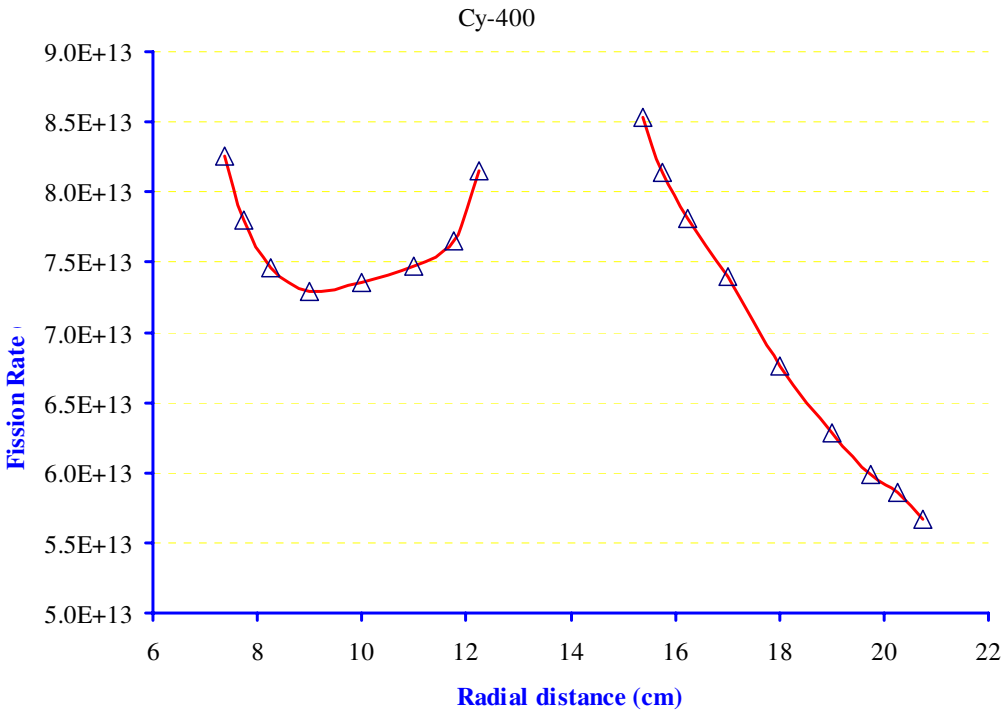

Fig. 41. Calculated fission rate [fissions/(cm^3*s)].

3.4 BENCHMARK RESULTS

The results of the final MCNP criticality calculations are shown in Table 11. These were calculated using the final model (HFV4.0). The final benchmarked values are as follow:

- The final estimated combined collision/absorption/track-length $k_{eff} = 1.00870 \pm 0.00013$.
- The final combined (col/abs/tl) prompt removal lifetime = $1.4369(10^{-4}) \pm 4.4797(10^{-8})$ seconds.
- The average neutron energy causing fission = 0.023304 ev.
- The energy corresponding to the average neutron lethargy causing fission = 0.16839 ev.
- The percentages of fissions caused by neutrons in the thermal, intermediate, and fast neutron ranges are:

  (<0.625 ev): 83.03% (0.625 ev – 100 kev): 15.50% (>100 kev): 1.48%

- The average fission neutrons produced per neutron absorbed (capture + fission) in all cells with fission was 1.7412.

- The average number of neutrons produced per fission was 2.439. Note that this value is slightly greater than the value used for source normalization (2.43) that is noted at the beginning of Sect. 3.3.

Table 11. Average k_{eff}, and 68, 95, and 99% confidence intervals

k_{eff} estimator	k_{eff}	Standard deviation	68% confidence	95% confidence	99% confidence
Collision	1.00866	0.00019	1.00847 to 1.00884	1.00828 to 1.00903	1.00816 to 1.00915
Absorption	1.00871	0.00013	1.00857 to 1.00884	1.00844 to 1.00897	1.00836 to 1.00905
Track length	1.00868	0.00020	1.00848 to 1.00888	1.00829 to 1.00907	1.00816 to 1.00920
col/abs/trk len	1.00870	0.00013	1.00857 to 1.00883	1.00844 to 1.00895	1.00836 to 1.00904

4. CONCLUSIONS

This document provided a thorough description and benchmarking results of the High Flux Isotope model HFV4.0. The MCNP model is a 3-D detailed and accurate representation of the HFIR cycle 400.

Benchmark calculations of eigenvalues, neutron fluxes, and reaction rates were performed using the model and compared with other published and or measured values. The comparison revealed that the model can accurately calculate reactor parameters with reasonable confidence. Users can easily modify the model input in any region, in order to incorporate future design changes, or experiments loading.

5. REFERENCES

1. X-5 Monte Carlo Team, *MCNP—A General Monte Carlo N-Particle Transport Code, Version 5*, LA-CP-03-0245, Los Alamos National Laboratory, April 24, 2003.

2. C. D. Harmon, R. D. Busch, J. F. Briesmeister, R. A. Forster, *Criticality calculations with MCNP A Primer*, L-I-12827-M, Los Alamos National Laboratory, August 1994.

3. L. L. Carter and R. A. Schwarz, *MCNP Visual Editor Computer Code Manual*, www.mcnpvised.com, September 2004.

4. D. E. Peplow, *A Computational Model of the High Flux Isotope Reactor for the Calculation of Cold Source, Beam Tube, and Guide Hall Nuclear Parameters*, ORNL/TM-2004/237, November 2004.

5. R. T. Primm III, *Reactor Physics Input to the Safety Analysis Report for the High Flux Isotope Reactor*, ORNL/TM-11956, Oak Ridge National Laboratory, 1992.

6. R. D. Cheverton and T. M. Sims, *HFIR Core Nuclear Design*, ORNL-4621, Oak Ridge National Laboratory, 1971.

7. J. C. Gehin, *HFIR Cold Source Review*, March 11, 1996.

8. S. C. Mo and J. E. Matos, *A Neutronic Feasibility Study for LEU Conversion of the HFIR*, Argonne National Laboratory.

9. S. C. Mo, N. A. Hanan, and J. E. Matos, "Comparison of the FRM-II HEU Design With an Alternative LEU Design," presented at the 1995 International Meeting on Reduced Enrichment for Research and Test Reactors, September 18–21, 1995, Paris, France.

INTERNAL DISTRIBUTION

1. E. D. Blakeman
2. J. A. Bucholz
3. S. E. Burnette
4. D. H. Cook
5. R. J. Ellis
6. M. B. Farrar
7. J. D. Freels
8. J. C. Gehin
9. R. W. Hobbs
10. D. J. Newland
11–14. R. T. Primm III
15. I. Remec
16. C. O. Slater
17. K. A. Smith
18. C. C. Southmayd
19–23. N. Xoubi
24. RRD Document Control Center

EXTERNAL DISTRIBUTION

25. H. D. Gougar, Manager, Fission and Fusion Systems, Idaho National Laboratory, P.O. Box 1625, MS 3860, Idaho Falls, ID 83415-3860
26. Dr. D. Kutikkad, University of Missouri Research Reactor Facility, Columbia, MO 65211
27. Dr. J. C. McKibben, University of Missouri Research Reactor Facility, Columbia, MO 65211
28. Dr. R. E. Williams, NIST Center for Neutron Research, 100 Bureau Drive, Stop 8560, Gaithersburg, MD 20899